Journal of Materials Chemistry C

ROYAL SOCIETY OF CHEMISTRY

REVIEW

View Article Online
View Journal | View Issue

Cite this: J. Mater. Chem. C, 2020, 8, 13482

Recent progress in chemical gas sensors based on organic thin film transistors

Mengge Wu,[ab] Sihui Hou,[a] Xinge Yu *[b] and Junsheng Yu *[a]

Received 2nd July 2020,
Accepted 4th August 2020

DOI: 10.1039/d0tc03132a

rsc.li/materials-c

Chemical gas sensors have important applications in the fields of environmental supervision, chemical pharmaceuticals, disease diagnosis and so on. With the rapid development of organic materials and device fabrication methods, research in organic thin film transistor (OTFT) based gas sensors has made significant progress and excellent sensing performances have been achieved. This review highlights recent progress in OTFT based gas sensors in the past several years, including the advances in typical sensing materials, interfacial engineering, and microstructure regulation. Furthermore, other developments in gas sensors such as application of new materials and integration of sensor arrays are also discussed in detail. This review aims at providing a comprehensive and fundamental understanding of OTFT based gas sensors, in terms of selection of sensing materials, functional thin film formation, the influence of interfacial properties and gas sensing mechanisms. And it is hoped that this will contribute to the fabrication of high-performance gas sensors and the development of related industries.

1. Introduction

Organic thin film transistors (OTFTs) have attracted enormous research interest due to their inherent advantages and wide potential for application in many fields.[1–10] Compared to traditional inorganic materials, organic semiconductors (OSCs) are superior in terms of materials design, light weight, mechanical flexibility and cost-effectiveness.[11,12] OSCs have great potential in the consecutive improvement and functionalization of sensing performances *via* the regulation of molecular structures, which is beneficial for achieving multifunctional integrated devices.[1,13] In addition, the rapid low-temperature annealing process of OSCs is compatible with printing technologies for large area and flexible electronics.[14–18] OTFT is a three

[a] State Key Laboratory of Electronic Thin Films and Integrated Devices, School of Optoelectronic Science and Engineering, University of Electronic Science and Technology of China (UESTC), Chengdu 610054, China. E-mail: jsyu@uestc.edu.cn
[b] Department of Biomedical Engineering, City University of Hong Kong, Hong Kong, China. E-mail: xingeyu@cityu.edu.hk

Mengge Wu

Mengge Wu received her BA degree and Master's degree from the School of Optoelectronic Science and Engineering at the University of Electronic Science and Technology of China (UESTC) in 2016 and 2019, respectively. She has been studying for her PhD at State Key Laboratory of Electronic Thin Film & Integrated Devices (SKLETFID) & UESTC since 2019. During 2020, she has been studying at the City University of Hong Kong (CityU) as a visiting PhD student under the supervision of Prof. Xinge Yu. Her main research interests are flexible photoelectrical devices such as nanogenerator, chemical sensors, and light-emitting diodes.

Sihui Hou

Sihui Hou received his Bachelor's degree from the School of Optoelectronic Science and Engineering at UESTC in 2016. Now, he is pursuing his PhD under the supervision of Prof. Junsheng Yu at UESTC, and his current research interests are organic thin-film transistors and their applications.

terminal device which consists of a OSC sensitive layer, a dielectric, source–drain electrodes and a gate electrode. According to the relative position of source–drain electrodes/gate electrode and OSC layer, OTFTs are divided into four categories, *viz.*, bottom-gate bottom-contact structure (BG/BC), bottom-gate top-contact structure (BG/TC), top-gate bottom-contact structure (TG/BC), and top-gate top-contact structure (TG/TC). An OTFT can be understood as an electrical switch that regulates the source–drain current (I_{DS}) through changing the gate voltage (V_G). When V_G is applied, the charge carriers will gather at the interface of the OSC layer/dielectric interface. If an appropriate voltage is applied to the source–drain electrodes (V_{DS}) at this time, carriers will flow between the source and drain electrodes forming the I_{DS}.

Based on the unique characteristics of OTFTs, the application of OTFT in gas sensors has attracted great attention.[19–24] The rapid development of organic semiconductors (OSCs) enables the development of low-cost OTFT sensors with the capability of real-time detection of toxic gases. The interaction between the analyte gas and OSCs can be converted into easy-to-read/record data. Responsivity (R), sensitivity (S), selectivity, response/recovery time, stability and limit of detection (LOD) are key parameters to quantify the sensing performance of a gas sensor. R is defined as the ratio of the change of an electrical parameter (usually the current in OTFT) to its initial value before and after exposure to the analyte gases. It can be calculated as follows:

$$R = \frac{\Delta Y}{Y_0} \times 100\% = \frac{Y_{Gas} - Y_0}{Y_0} \times 100\% \quad (1)$$

where ΔY represents the variable quantity of electrical parameter, Y_0 means the initial value and Y_{Gas} is the value after exposure to analyte gases. S is defined as the slope of the linear relationship between responsivity and the gas concentration, which can be calculated using the following equation, and the unit is % ppm^{-1} or % ppb^{-1}.

$$S = \left.\frac{\partial R}{\partial c}\right|_{lin} \quad (2)$$

where c denotes the gas concentration. Selectivity is used to identify whether the sensor can still distinguish the analyte gas in the presence of interferents. Response time is defined as the time of current increase from I_{off} to (I_{off} + 90% × ΔI), and recovery time refers to the time of current recovery from I_{on} to (I_{off} + 10%×ΔI), where $\Delta I = I_{on} - I_{off}$, I_{off} and I_{on} are the initial current with no exposure to analyte gas and saturation current upon exposure to analyte gas, respectively. Stability usually involves operation stability and environmental stability in gas sensors. LOD in gas sensors is typically used as a predictor of the detection limit, where the concentration of the gas analyte is assumed to be detectable. Prominent advances have been achieved in the last several decades, and the sensor performance has been boosted significantly, with a sensitivity of over 1000%/parts per million (% ppm^{-1}),[20,25] response and recovery time at the seconds level,[26,27] and a LOD as great as parts per billion (ppb).[25–28]

In this review, we aim at providing a systematic survey of the recent advances in designing and exploring OTFT based gas sensors with excellent performance, from sensitive materials, to interfacial engineering, to microstructure regulation of OSC, and to the integration strategy of sensor arrays. Chemical gas sensitive materials are the key to realizing gas sensors. In Section 2, we review the recent progress in the sensitive materials and the corresponding sensing mechanisms that have been used in OTFT sensors. Interfacial properties in OTFT play an important role in the gas sensing performance; therefore, interfacial engineering is an efficient route to enhance the performance of sensors. In Section 3, we review the recent progress of OTFT based gas sensors from the perspective of interfacial engineering, including modifications in the related interfaces and efforts made in changing the chemical and physical properties at the interfaces using novel methods. Microstructure regulation in OSC layers *via* different techniques is discussed in Section 4. Other important studies, such as exploring biomaterials as dielectric and developing sensor arrays are summarized in Section 5. The conclusion of this paper and outlook in terms of further research prospects are discussed in Section 6.

Xinge Yu

Xinge Yu is an Assistant Professor of Biomedical Engineering at CityU. He finished his PhD research of printable flexible electronics at Northwestern University (NU) and UESTC in 2015. From 2015 to 2018, He was a postdoctoral associate in the Center for Bio-Integrated Electronics at NU and the Department of Materials Science and Engineering at the University of Illinois at Urbana-Champaign. His research focuses on developing skin-integrated electronics and bioelectronics, and he conducts multidisciplinary research addressing challenges in practical applications.

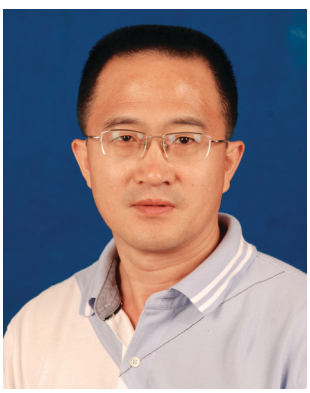

Junsheng Yu

Junsheng Yu completed his PhD at the Graduate School of Bio-Applications & System Engineering at Tokyo University of Agriculture and Technology in 2001. He is a Professor of SKLETFID & UESTC majoring in organic photoelectronic and electronic materials and devices. Furthermore, he is the director of Sichuan Province Key Laboratory of Display Science and Technology. His research focuses on developing organic photoelectric devices such as organic/perovskite light-emitting diodes, organic/perovskite solar cells, organic/perovskite photodetectors and organic sensors based on thin film transistors.

2. Chemically sensitive materials

Charge transport in OSCs happens between molecules *via* the conjugated π bonds, which shows great relevance to the external environment and thus makes them serve as gas sensors.[29] Organic materials based gas sensors typically work in the following steps: (i) the gas molecules (analytes) adsorb onto the surface of the OSC thin film; (ii) the analytes diffuse into the bulk OSC thin film; and (iii) the analytes vary the charge transport properties of the OSC thin film either in a physical absorption such as dipole–dipole interaction *via* van der Waals forces, or through a chemical reaction such as hydrogen bonding and electrostatic interactions.[27,30–35] The essential difference between physical absorption and chemical interaction lies in whether there are new substances produced. Generally, gas sensors based on physical absorption can be used repeatedly, while some sensors based on chemical interactions can be used only once due to the irreversibility of the chemical reactions. The properties of OSCs such as chemical structures, charge transfer capabilities, and functional groups as well as the film morphologies determine the sensing performance significantly.[36–38] So, the key to the success of organic gas sensors is to realize an obvious correlation between electrical properties and analyte gases. For instance, the design of sensing materials into a porous film can facile gas diffusion into the bulk film for enhancing the absorption amount of the gas analytes[39,40] or to explore sensing materials to form certain molecular structures with specific recognition functional groups for targeting gases.[41,42]

Similar to inorganic semiconductors, OSCs can be divided into p-type and n-type, where p-type represents hole-dominated transport and n-type represents electron-dominated transport. Typically, oxide gases, such as NO_2, O_2, Cl_2 *etc.* can lead to a conductivity enhancement for the p-type OSCs, while reductive gases such as NH_3, H_2S, H_2 *etc.* often cause a conductivity decrease. On the contrary, the conductivity of n-type OSCs mostly represent opposite response behaviours to gases that are of p-type OSCs. According to the molecule structures, OSCs can be divided into small molecules and polymers. Small molecules mostly relies on physical vapour deposition and exhibit the advantages of high purity and crystallization controllability, while polymers are typically cast *via* solution routes and are more suitable for large area processing. Table 1 summarizes the representative high performance OTFT based gas sensors reported in recent literature. Fig. 1 and 2 sum up the chemical structures of polymers and small molecules mentioned in this review, respectively.

2.1 Polymer OSCs as sensitive layers

Polythiophene and its derivatives are the most reported p-type polymer OSCs for gas sensors due to their simple material synthesis processes (Fig. 1a). Poly(3-hexylthiophene) (P3HT) as a representative material has been widely used in OTFT based gas sensors for many years.[56–59] Taking the sensing of a typical harmful gas ammonia (NH_3) as an example, the interaction between P3HT and NH_3 can reduce the density of hole carriers, leading to a decrement of conductivity in the P3HT channel and thus present a response to NH_3 *via* current decrease and the threshold voltage shifts. As Seohyun *et al.* reported, the LOD of P3HT single crystal nanowire on NH_3 can lower to 8 ppb.[28] Doping functional materials such as metal oxides and polymers in P3HT thin films enables changing of the microstructures in the sensing layer and thus improves sensitivity. A detailed discussion of the corresponding studies can be found in the following sections. Poly(9,9-dioctyl-fluorene-*co*-bithiophene) (F8T2) is another typical polythiophene derivative that is often used to detect specific organic vapours, *i.e.* acetone and ethanol. F8T2 contains fewer polarity branches than P3HT, which improves the selectivity. However, the low sensitivity of F8T2 is a problem, since only a small amount of gas analytes can adsorb onto the F8T2 thin film due to weak van der Waals forces. Introducing functional groups into F8T2 can improve the sensitivity. A successful example reported by Kim *et al.* involved combining F8T2 with oleylamine-modified graphene oxide (OA-GO), where OA-GO was used to enhance the interaction with the analyte gas.[31] Poly(bisdodecylquater thiophene) and poly-(bisdodecylthioquater thiophene) (PQT12 and PQTS12,

Table 1 High-performance OTFT based gas sensors reported in recent years

Target gases	Material	Sensitivity	LOD	Response/recovery time	Ref.
NO_2	TIPS-pentacene	1329% ppm^{-1}	1.93 ppb	10 min/>20 min	25
	DPP-fluorene-based polymer	614% at 20 ppm	0.5 ppm	5 min/~3 min (40 °C)	43
	TIPS-pentacene	1181% ppm^{-1}	20 ppb	200 s/400 s	44
	CuPc	160 000% at 30 ppm	400 ppb	400 ppb	45
	PQTS-12	410% at 5 ppm	1 ppm	15 min/—	46
NH_3	P3HT nanowire	~220% at 5 ppm	8 ppb	N/A	28
	PDFDT	56% at 10 ppm	1 ppm	>180 s	34
	DNTT	340% ppm^{-1}	10 ppb	95 s/200 s	39
	Pentacene/gelatin	17.6% at 0.5 ppm	174.0 ppb	15.4 s/42.2 s	47
	P3HT–DPPCN	53% at 0.5 ppm	0.5 ppm	5 min/5 min	48
	CoPc + TPFB	63% at 4.5 ppm	0.35 ppm	90 s/—	49
	pDPPBu-BT	45% at 10 ppm	10 ppb	5 s/—	50
	P3HT–PMMA	1481% at 30 ppm	0.7 ppb	N/A	51
DMMP	F_{16}CuPc	10^6% ppm^{-1}	<5 ppm	20 min/180 min	52
	6PTTP6	70% at 5 ppm	~10 ppb	40 s/—	53
SO_2	CuPc nanowire	764% at 20 ppm	0.5 ppm	3 min/8 min	54
H_2S	BDFTM	11% at 0.1 ppm	10 ppb	5 s	27
	Spirobifluorene-based polymer	95% at 1 ppm	1 ppb	15 s/—	55

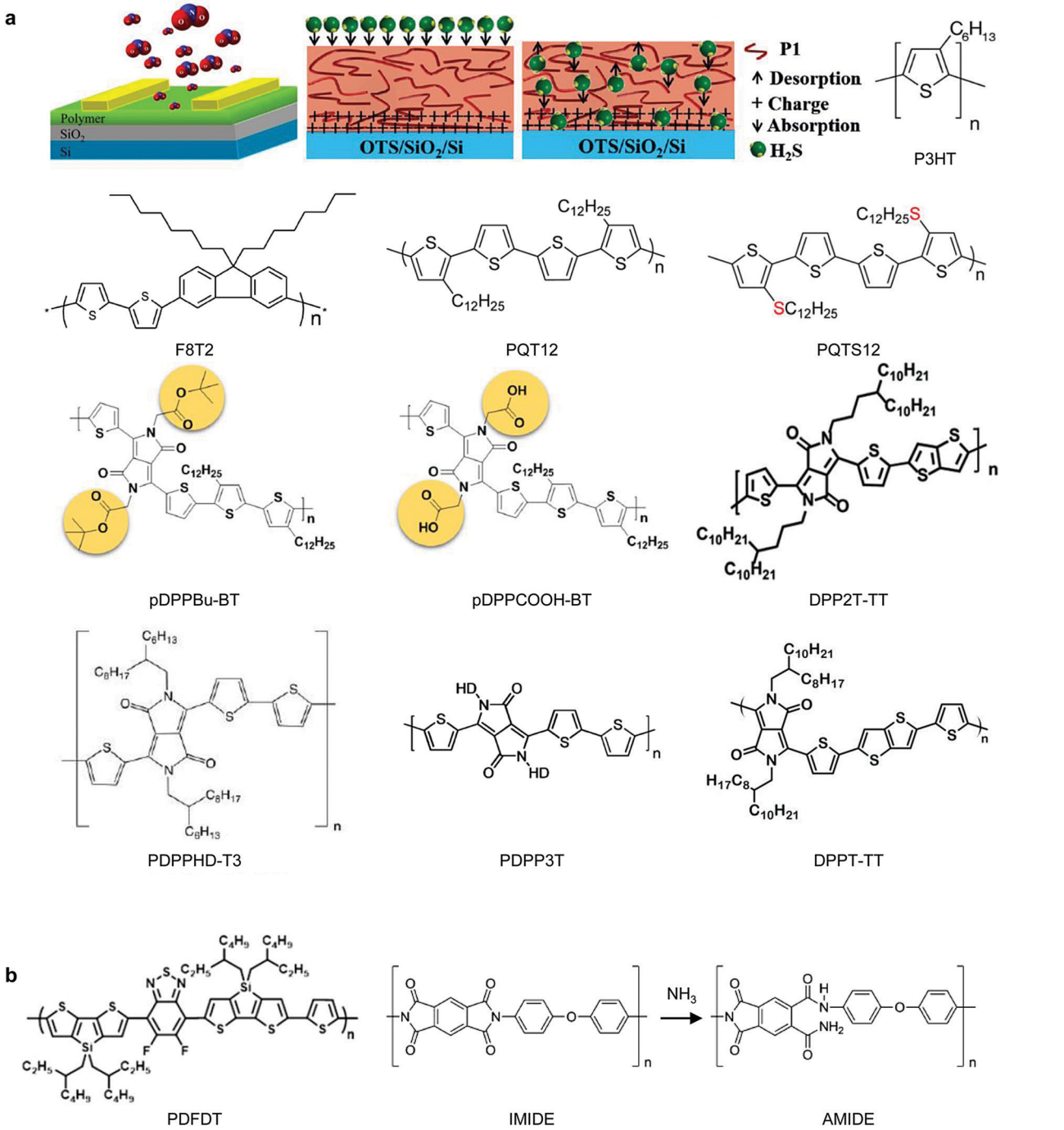

Fig. 1 Chemical structures of polymer OSCs mentioned in this review. (a) The schematic illustrations of physical adsorption of OTFT sensors and some representative polymers. (b) A polymer with a chemical reaction response mechanism. Adapted with permission from ref. 31, 50, 55, 60, 61 and 63–66, respectively. Copyright 2017 American Chemical Society, 2016 Wiley, 2014 The Royal Society of Chemistry, 2016 American Chemical Society, 2017 Wiley, 2016 Wiley, 2009 American Chemical Society, 2016 Wiley, 2017 American Chemical Society and 2016 The Royal Society of Chemistry.

respectively) are two other sensing materials worth mentioning, which contain sulphide groups serving as functionalized analogue adjacent to thiophene rings. The sulphide groups can increase the trap density and enhance the redox interactions between OSCs and gas analyte molecules.[46]

Diketopyrrolopyrrole (DPP)-based conjugated polymers have received increasing attention in recent years, and have been applied in high-performance NH_3 sensors. As reported by Khim *et al.*, poly[[2,5-bis(2-octyldodecyl)-2,3,5,6-tetrahydro-3,6-dioxopyrrolo[3,4-*c*]pyrrole-1,4-diyl]-*alt*-[[2,2′-(2,5-thiophene)bis-thieno(3,2-*b*)thiophene]-5,5′-diyl]] (DPPT-TT) showed a pronounced response to NH_3, and a high sensitivity of 82% to 10 ppm NH_3 gas when deployed in OTFT as the sensing layer based with a thickness of 2 nm.[60] Meanwhile, the DPPT-TT based sensors

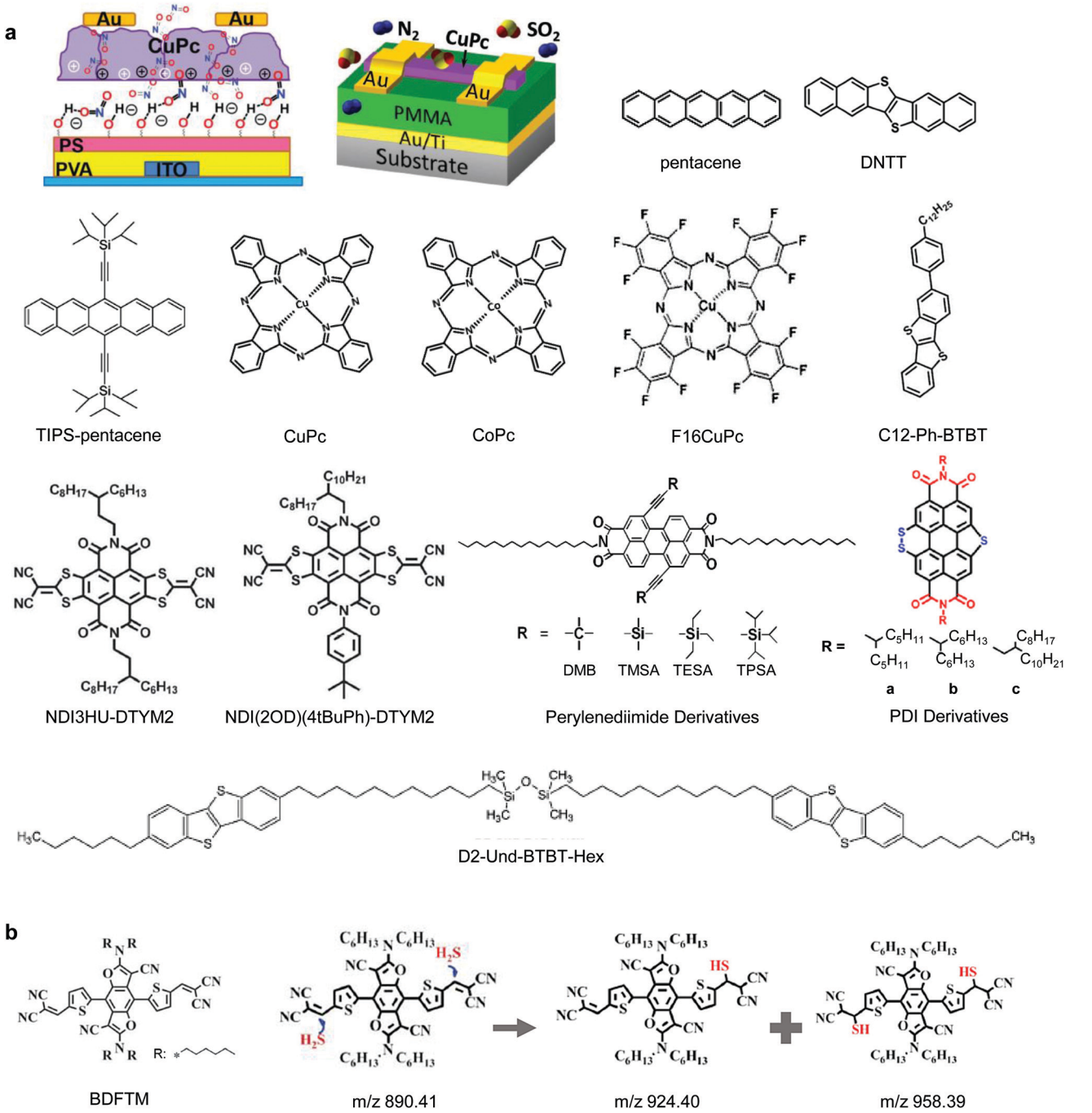

Fig. 2 Chemical structures of the small molecule OSCs mentioned in this review. (a) The schematic of physical adsorption and small molecules involved. (b) Small molecules with the sensitive mechanism of chemical reaction. Adapted with permission from ref. 20, 27, 38, 39, 44, 52, 84, 85, 97–99 and 122, respectively. Copyright 2017 Wiley, 2013 Wiley, 2019 The Royal Society of Chemistry, 2017 Wiley, 2017 Wiley, 2009 American Institute of Physics Publishing, 2016 Wiley, 2013 Wiley, 2015 The Royal Society of Chemistry, 2019 The Royal Society of Chemistry, 2018 The Royal Society of Chemistry and 2014 Wiley.

also exhibited obvious responses to ethanol (1000 ppm) and ethylene vapours (1000 ppm). pDPPBu-BT is another representative DPP polymer for gas sensing, in which the *tert*-butoxycarboxyl groups incorporated in the side chains can convert groups to carboxyl groups (–COOH) by thermal annealing treatment.[26] As a result, the annealed pDPPBu-BT film exhibits a rapid response ability towards NH_3 and better selectivity to other volatile gases such as CH_2Cl_2, hexane and ethyl acetate.[26] Other DPP derivatives such as poly(diketopyrrolopyrrolethiophene-thieno[3,2,*b*]thiophene-thiophene) (DPP2T-TT) are also sensitive to gases.[61] Moreover, introducing nano-porous structure into the DPP based thin film can significantly improve the sensor performance, and an ultrafast response to NH_3 of below 1 ppb at a sub-second time level can be achieved.[61] Besides the p-type DPP derivatives

mentioned above, there are many ambipolar DPP derivatives that can conduct both holes and electrons. Therefore, ambipolar DPP derivatives are promising candidates for high selectivity gas sensors due to the diverse sensing parameters from both n-type and p-type OTFTs. Ambipolar poly(diketopyrrolopyrroleterthiophene) (PDPPHD-T3) exhibites balanced mobility for both holes and electrons due to the additional planarity induced by unsubstituted terthiophene units between each pair of DPP derivatives.[62,63] Combining the changes in both hole and electron mobilities, the PDPPHD-T3 based gas sensor can identify xylene isomer vapors easily.

Besides the physical adsorption sensing mechanism in the above-mentioned polymers, chemical interaction is another important sensing mechanism in polymers. For instance, as exhibited in Fig. 1b, the sensing mechanism of the poly(4-(4,4-bis(2-ethylhexyl)-4*H*-silolo-[3,2-*b*:4,5-*b*′]dithiophen-2-yl)-7-(4,4-bis(2-ethylhexyl)-6-(thiophen-2-yl)-4*H*-silolo[3,2-*b*:4,5-*b*′]dithiophen-2-yl)-5,6-difluorobenzo[*c*][1,2,5]thiadiazole) (PDFDT) polymer to NH_3 is that fluorine atoms in PDFDT interact with hydrogen atoms in NH_3 by weak hydrogen bonds and electrostatic interactions, thus changing the hole transport behaviour *via* lowering of the HOMO level of PDFDT.[34] In Benjamin *et al.*'s report, the PDFDT gas sensors could achieve a LOD as low as 1 ppm and a sensitivity of 56% to 10 ppm NH_3. In addition, polyvinyl alcohol formaldehyde (PVF)-based composites of PVF-coumarin-6 (PVFCOU) can form $PVFCOUSO_2$ through chemical reaction with SO_2 and the occurrence of chemical interactions between PVFCOU and SO_2 are mainly manifested in the stretching frequency shifts of PVFCOU and $PVFCOUSO_2$ in their FT-IR spectra.[35] As a result, an ultrafast response time of 3 s for 400 ppb SO_2 and LOD of as low as 115 ppb were achieved. Besides, the polyimide (IMIDE) reacts with NH_3 and forms amides (AMIDE), achieving an efficient sensor with the molarity lowered to 3.5 mM.

2.2 Small molecule OSCs as sensing layers

Small molecule OSCs are widely used in OTFT based gas sensors due to the advantages of material purity, controllable crystallization, chemical stability and higher mobility than that of most polymers. However, the deposition method for small molecule OSCs are typically physical vapour based, which limits the manufacturing of large-area sensor arrays.[67] Furthermore, the microstructures of small molecule OSCs are basically polycrystalline based, which also raises problems of uniformity and flexibility.[68]

Due to the well-organized molecular arrangement behaviours, pentacene and its derivatives exhibit high mobility and structural stability.[38,69–72] The earliest report on a pentacene-based gas sensor was presented by Takashi Minkata and a reversible LOD of 0.2 ppm for NO_2 gas was achieved, which revealed the application potential for detecting oxidizing gases in air.[73] In 2014, Misbah *et al.* reported a novel monolayer pentacene-based gas sensor to detect NH_3, with a LOD of 10 ppm which is more sensitive than a conventional sensor with a 50 nm pentacene layer.[36] Typical pentacene based gas sensors have been thoroughly studied, and thereby researchers have combined new functional materials with pentacene to fabricate high-performance biocompatible gas sensors in recent years. Taking the study of Shi *et al.* as an example, the negatively charged phosphate groups in DNA could adsorb more NO_2 molecules at the dielectric/pentacene interface compared to a sensor without DNA. As a result, the responsivity of the DNA/pentacene device improved by an order of magnitude.[74] Furthermore, guanine was also applied in pentacene based gas sensors, and the sensing mechanism of guanine to NO_2 is that the amino group ($-NH_2$) and imino groups (–NH) in guanine can adsorb NO_2 molecules.[71] Therefore, the sensitivity was improved and the detection limit decreased to 1 ppm. Shi's research studies provide new ideas for fabricating high-sensitive pentacene gas sensors. 6,13-Bis(triisopropylsilylethynyl)pentacene (TIPS-pentacene) is one of the most used pentacene derivatives in OTFTs for gas sensors, and the TIPS-pentacene response to gases is through a physical adsorption mechanism.[25,44,75] Wang *et al.* reported an ultrasensitive NO_2 sensor based on TIPS-pentacene, and the device achieved a sensitivity of 1000% ppm^{-1} and detection limit lowered to 20ppb.[44] The effect of TIPS-pentacene thickness on the responsivity was studied, and results demonstrated that the reason for the best performance of the thinnest 5 nm device is that ultrathin films can combine small original charge carrier concentration and efficient charge transport, thus realizing an obvious change in carrier density. In addition, Zhuang *et al.* reported nanofibrillar structured TIPS-pentacene *via* an orthogonal/parallel off-center spin-coating method; as a result, TIPS-pentacene films with highly aligned conjugated backbones and well-regulated potential barriers at grain boundaries were obtained.[76] Upon exposure to NO_2, the interactions of TIPS-pentacene and analyte occurred and then effective charge carriers were released at grain boundaries due to the reduced potential barriers induced using an off-center process, leading to enhancement in carrier mobility. In consequence, I_{on} values show a variation of about 32.9% and 52.7% under 1 ppm NO_2 for orthogonal and parallel devices respectively, which are higher than that of 2.3% for an on-center device.

Phthalocyanines (Pcs) are well known small molecule OSCs due to their good chemical and physical stability, which have been widely used in OTFT based gas sensors. In 1987, research on the response of five kinds of phthalocyanines to oxidizing gases was reported by Laurs and Heiland.[77] The results revealed that the conductivity of p-type Pc increased obviously upon exposure to gases with high affinity (such as I_2 and Br_2), which is over the O_2-induced level. The most frequently-used Pc materials applied in gas sensors are copper(II) phthalocyanine (CuPc,)[20,78–80] and cobalt(II) phthalocyanine (CoPc),[37,81] and the molecular structures are displayed in Fig. 2a. To further boost the sensing properties, various treatment methods have been devoted to the Pc based OTFT sensors based on different sensing mechanisms.[80] For instance, Huang *et al.* demonstrated NO_2 gas sensors based on CuPc with a limit of detection of 400 ppb and maximum sensitivity of 160 000% by simple UV–ozone treatment of polymer dielectrics.[20] UVO treatment induces many polar carbon–oxygen functional groups at the

dielectric surface, leading to more NO_2 molecules being adsorbed *via* van der Waals forces. Song *et al.* pointed out the selective transferability of gas sensors with dinaphtho[3,4-*d*:30,40-*d*0]benzo[1,2-*b*:4,5-*b*0]dithiophene (Ph5T2) modified CuPc.[82] The so-called selective transferability is that unmodified CuPc sensors exhibited a stronger response to H_2S, while modified CuPc sensors showed a greater response to N_2O. Under the same test conditions, the former's response to 10 ppm H_2S reached 1088% while 10 ppm NO_2 was only 97.5%, in contrast, the latter's response to H_2S reduced to 234% while that to NO_2 increased to as high as 460%. Kumar *et al.* decorated reduced graphene oxide (rGO) with unsubstituted CuPc to enhance the Cl_2 sensing performance, which was attributed to the synergetic effects of the higher number of interaction sites in CuPc and the conductive network induced by rGO.[79] In addition to CuPc, CoPc has been also studied and various strategies have been adopted to form high-quality CoPc for high-performance gas sensors. In 2019, Kaya *et al.* synthesized a new CoPc sensor with 5-(trifluoromethyl)-2-mercaptopyridine and it showed enhanced NH_3 performance in terms of a LOD of 0.3 ppm and fast response/recovery rate.[37] Moreover, this CoPc gas sensor displays excellent selectivity to NH_3 even though volatile organic vapors are present in the gas mixture. All these advances provide new ideas for the precise detection of mixed gases.

The co-oligomers of benzene and thiophene have the advantages of ultrahigh mobility, air stability and thermal-oxidative stability and have thus attracted attention and have been used in gas sensors. Typical benzene/thiophene co-oligomers are alkyl derivatives of benzothieno[3,2-*b*][1]benzothiophene (BTBT),[83–87] dinaphtho[2,3-*b*:2′,3′-*f*]thieno[3,2-*b*]thiophene (DTNN),[39,88] and dithieno[2,3-*d*;20,30-*d*0]benzo[1,2-*b*;4,5-*b*0]dithiophene (DTBDT).[30,89,90] In 2011, Minemawari *et al.* synthesized 2,7-dioctyl[1]benzothieno[3,2-*b*][1]benzothiophene (C_8-BTBT) single crystals *via* anti-solvent crystallization and inkjet printing, obtaining a high mobility of 16.4 $cm^2\ V^{-1}\ s^{-1}$.[83] Afterwards, He *et al.* demonstrated a high performance OTFT based monolayer of C_8-BTBT with a hole mobility as high as 30 $cm^2\ V^{-1}\ s^{-1}$.[91] An interesting phenomenon in 2-(4-dodecyl phenyl)[1]benzothieno[3,2-*b*]benzothiophene (C_{12}-Ph-BTBT) was found, in which C_{12}-Ph-BTBT showed a bilayer structure after annealing and a mobility of up to 8.7 $cm^2\ V^{-1}\ s^{-1}$.[84] Trul *et al.* developed a new BTBT organosilicon dimer of α,α′-dialkylquaterthiophene (D2-Und-BTBT-Hex, as shown in Fig. 2a) and explored the conditions of fabricating low-defect D2-Und-BTBT-Hex monolayers.[85] The OTFT based on D2-Und-BTBT-Hex achieved great performance with a mobility of $7 \times 10^{-2}\ cm^2\ V^{-1}\ s^{-1}$ and an I_{on}/I_{off} of 10^5. Furthermore, the D2-Und-BTBT-Hex OTFT also showed a great response to NH_3 with a LOD of 400 ppb. Since the conduction channel of OTFT is only a couple of nanometers along the dielectric surface, thus shortening the diffusion distance from the surface of the OSCs to the conductive channel is critical. Lu *et al.* reported using the versatile template method to deposit ultrathin micro-porous OSC films of dinaphtho [2,3-*b*:2′,3′-*f*]thieno[3,2-*b*]thiophene (DNTT) for the gas sensor, yielding a high sensitivity of 340% ppm^{-1} to NH_3 and a LOD at the ppb level.[39] Werkmeister *et al.* investigated the influence of a DNTT film morphology on the response time of NH_3, and the results showed that the fastest response was achieved from the Volmer–Weber 3D structure.[88] To help understand the sensing mechanism in many OTFT based gas sensors, Zhou *et al.* studied the recovery behaviours of gas sensors based on *n*-nonanyl substituted DTBDT (DTBDT-C9) in N_2 and in air. The results illustrated that, different with the conventional simple absorption/desorption process, H_2O pre-doped in DTBDT-C9 film before NH_3 absorbed and H_2O re-doped in DTBDT-C9 film when NH_3 desorbed, respectively.[30]

The advance in n-type OSCs is limited due to their low mobility and instability in air, while the stability of the n-type materials can be improved *via* incorporation of electron withdrawing groups such as cyan groups (CN^{-1}), fluorine ions (F^{-1}) and chloride ions (Cl^{-1}) on their backbones or side chains. Two kinds of representative n-type OSCs, perylene diimide (PDI)[92] and naphthalene diimide (NDI)[93–96] derivatives are the most reported for gas sensors of NH_3, NO_2 and some volatile organic compounds. The performance of PDI is comparable with most p-type OSCs, and therefore it is regarded as one of the most promising n-type OSCs. Liu *et al.* reported alkyl and fluoroalkyl substituted core-tetrachlorinated perylene diimides (4ClPDI) with a mobility of up to 1.43 $cm^2\ V^{-1}\ s^{-1}$ and I_{on}/I_{off} of 10^4.[92] In 2000, the earliest NDI derivative of *H*,*H*-NDI-$CH_2C_7F_{15}$ was reported by Katz *et al.*, which had a mobility of 0.1 $cm^2\ V^{-1}\ s^{-1}$ and a high I_{on}/I_{off} of 10^5.[93] Zang *et al.* discovered an interesting phenomenon of NDI derivatives (NDI(2OD)(4tBuPh)-DTYM2) using a gas-phase reaction assisted detection method. Effective adsorption of NH_3 on NDI(2OD)(4tBuPh)-DTYM2 occurred and the increased change in I_{DS} was not reversible. Next, when HCl gas exposured to this NH_3-adsorbed sensor, I_{DS} decreased obviously and recovered to device's initial level when none gas exposed. The reason can be attributed to the de-adsorption process of NH_3 enabled by the NH_4Cl nanoparticles (formation due to the chemical interaction between HCl and NH_3 absorbed).[95] As a result, the adsorption of NH_3 on the NDI(2OD)(4tBuPh)-DTYM2 sensitive layer assisted the precise detection of HCl gas.

Most small molecule OSCs respond to analyte gases mainly *via* physical adsorption (trapping or doping process), while there are still some small molecules that are gas sensitive through chemical reactions. Generally, the selectivity of OTFT sensors obtained *via* chemical reactions is better than those of physically adsorbed ones because of the targeting behaviours for specific gases in chemical reactions. However, the recovery characteristics of OTFT sensors based on chemical reaction are a problem since most of the chemical reactions are irreversible. Luo *et al.* reported a new cruciform donor–acceptor molecule 2,2′-((5,5′-(3,7-dicyano-2,6-bis(dihexylamino)benzo[1,2-*b*:4,5-*b*′]difuran-4,8-diyl)bis(thiophene-5,2-diyl))bis(methanylylidene))dimalononitrile (BDFTM) that can detect H_2S.[27] And the reaction mechanism of BDFTM to H_2S is presented in Fig. 2b, which illustrates that the selective sensing of H_2S with BDFTM derives from the Michael addition of H_2S to the 2-methylenemalononitrile groups in BDFTM. Therefore, comparing the responses to H_2, CO_2, and NH_3, BDFTM based gas sensors showed obvious decrement of I_D for low concentration H_2S under

the same detection conditions, and achieved high sensitivity with a detection limit down to 10 ppb. However, due to the irreversible chemical reaction, this BDFTM-based gas sensor cannot be reused.

3. Interfacial engineering

As Nobel laureate Herbert Kroemer said "The interface is the device".[100] The interface plays important roles in the growth of OSCs and the injection/transport of carriers in the bulk and at the surface. There are three interfaces in conventional BGTC OTFTs: the gate electrode/dielectric interface, the dielectric/OSC interface, and the OSC/D–S electrode interface. Among them, the dielectric/OSC interface is the most important one because the effective conductive channel is in several single-molecule layers (several nanometers) of the OSC layer on top of the dielectric. Compared to inorganic materials, organic materials can't form real energy bands due to the weak intermolecular forces. For this reason, the migration of charge carriers in organic materials is realized by hopping.[101] Therefore, to know the effect of the dielectric/OSC interface on the performance of gas sensors, many perspectives need to be taken into account. At the same time, the OSC/D–S electrode interface is also an important research topic, since it is related to the injection and transport of charge carriers. Factors affecting the quality of the OSC/D–S electrode interface are mainly determined by the energy gap and the contact resistance between OSC and D–S electrodes. The closer the Fermi level of the metal electrode to the Highest Occupied Molecular Orbital (HOMO) energy level of p-type OSC or the Lowest Unoccupied Molecular Orbital (LUMO) energy level of n-type OSC, the more effective the carrier transport that could happen in OTFTs.[102] Over the past decade, extensive efforts have been devoted to the interfacial engineering in OTFT-based gas sensors, including chemical modifications such as growing covalently bonded self-assembled monolayers (SAMs) or physical modification methods such as insertion of a thin buffer layer at the specific interface. In this section, we summarize and analyse the recent studies of interfacial engineering in OTFT based gas sensors.

The dielectric/OSC interface determines the crystallization of OSC and charge transport at this interface.[103,104] The chemical and physical properties of the dielectric have a huge influence on the crystallization of OSCs.[105] For instance, the surface energy of the dielectric is closely related to device mobility.[106] By comparing the surface morphology of OSC thin films, it is found that the grain size of the OSCs is likely to change with the surface energy of the dielectrics. M. Yoshida and F. S. Kim studied the crystallinity of OSCs on different dielectrics including PMMA, PS and PVA and found that the morphologies were obviously different, leading to a dramatic variation of the gas sensing performance.[107,108] Interfacial traps act as scattering centres and trap the hole/electron carriers, resulting in the decrement of sensing performance. In this regard, reducing the density of traps that are located at the dielectric/OSC interface by interfacial engineering is an effective way to improve the charge transport. Interfacial engineering for a dielectric/OSC interface using various modification methods provides an important and effective way to improve the crystallization and the charge transport, and thus promoting the sensing performance of a gas sensor. Next, we will describe the efforts devoted to interface engineering in terms of improving the crystallization and charge transport.

Dielectric modification is a common strategy for tuning the surface energy of a dielectric/OSC interface. To date, polymers, small molecule and metal oxides have been used as modification layers for dielectrics. For example, Sun *et al.* used small molecules of *para*-hexaphenyl (p-6P) as the modification layer between SiO_2 and α-sexithiophene (α-6T), as displayed in Fig. 3a.[104] The results showed that the α-6T film on the p-6P/SiO_2 substrate was more continuous with a larger grain size of α-6T than that of those on the bare SiO_2 surface. The corresponding p-6P modified OTFT sensors exhibit a great sensitivity of 998% ppm^{-1} and a low detection limit of 1 ppm. As shown in Fig. 3b, Shao *et al.* studied the effect of processing solvents (including chlorobenzene, dichlorobenzene, toluene and *o*-xylene) on the crystallinity of TIPS-pentacene, which was mainly reflected in the effect on the balance between crystallinity and the density of grain boundary.[25] The results demonstrated that the TIPS-pentacene thin film formed from *o*-xylene solution exhibited the best NO_2 response, in terms of a detection limit of 1.93 ppb and sensitivity with 60-fold improvement over that of 274.8%. As shown in Fig. 3c, polymers having methyl cellulose (MC) as the modification layer are introduced to control the crystallization of pentacene to provide more trap sites, resulting in enhanced gas responsivity (detection limit of 1 ppm for NO_2).[38] According to AFM images and impedance spectroscopy, it was found that the MC layer not only controlled the growth of OSCs, but also induced electrostatic interactions with NO_2 *via* its dipole alignment. A SAM is a kind of 2D material with a highly ordered structure formed on various surfaces spontaneously, and has been used to modify dielectrics to control the crystallization of OSCs.[103,109] One of the most well-known embodiments is the surface modification of SiO_2 with *n*-octadecyltrichlorosilane (OTS) or hexamethyldisilazane (HMDS), which enables creation of a covalently bonded surface with tuned surface energy for improving the crystallization of OSCs. Considering dielectric modification in OTFT sensors, creating additional trapping sites that can interact with the analyte gases is an effective route. Han *et al.* reported a high-response NO_2 gas sensor with the ZnO nanoparticles/PMMA hybrid dielectric, as shown in Fig. 4a.[110] The ZnO nanoparticles acting as impurities embedded in a PMMA layer increased the surface energy of the mixed dielectric and thus played the roles of both reducing the grain size of pentacene and enlarging the depth of grain boundaries of a CuPc sensing film. The high electron affinity of NO_2 allowed interaction with both CuPc and ZnO nanoparticles, resulting in enhanced variation of saturated current and carrier mobility upon exposure to NO_2. Based on a similar strategy, polymers with hydroxyl dipoles, such as PVA have also been proved to be an effective modification layer, since the hydroxyl dipoles can reorient

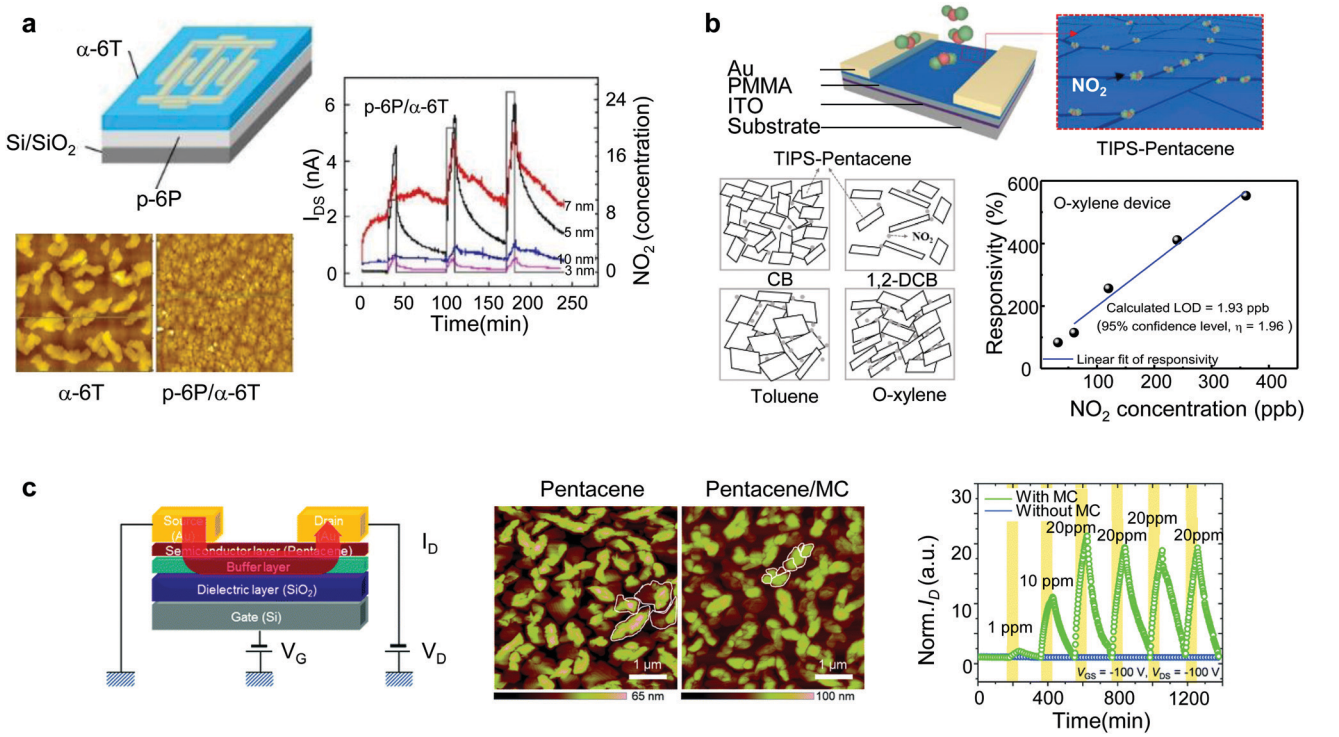

Fig. 3 Examples of adjusting the OSC crystallization *via* interfacial engineering mentioned in this review. (a) A small molecule of p-6P was introduced into the SiO_2/α-6T interface. On the top left is the schematic of the device structure, on the bottom left is the AFM images of α-6T films without and with p-6P underlayer, and on the right is the I_{DS}–time–NO_2 concentration response performance curves of a p-6P/α-6T based gas sensor. (b) Organic solvent selection method used in a TIPS-pentacene based NO_2 gas sensor to regulate the crystallization of TIPS-pentacene. On the top is the schematic of the device structure, on the bottom left is the crystallization schematic of four TIPS-pentacene films, and on the bottom right is the responsibility–NO_2 concentration curve of the *O*-xylene device. (c) Polymer of methyl cellulose (MC) as the interlayer to improve the crystallinity of pentacene. On the left is the schematic of the device structure, in the middle is the AFM images of pentacene without and with an MC interlayer, and on the right are the normalized I_D–time response curves. Adapted with permission from ref. 104, 25 and 38, respectively. Copyright (a) 2019 Elsevier, (b) 2019 The Royal Society of Chemistry, (c) 2019 The Royal Society of Chemistry.

under a gate bias, which creates new trapping sites for charge carriers and leads to electrical property responses to gas analytes. Interestingly, bio-inspired or bio-compatible materials can also serve as modification materials for OTFT sensors. Shi *et al.* reported the introduction of a thin DNA layer as modification on top of a PMMA dielectric by spray coating, as shown in Fig. 4b.[74] Due to the strong interaction between oxidative NO_2 molecules and the reductive phosphate groups in DNA molecules these OTFT sensors exhibited much greater sensitivity than the sensors without DNA modifications. Other bio-materials that are inbuilt with polarization functional groups (such as C–O, C═C, C═O, –NH and –OH) can also serve as functional modification layers or even dielectric layers for OTFT sensors.[47] These functional layers can interact with gas analytes, and fetter free charge carriers, which offers a new idea for the selection of dielectric materials. In addition, poly(vinyl alcohol) (PVA) was utilized as a gas accumulation layer, in which PVA could adsorb/desorb NH_3 when an electrical field was applied or removed, as exhibited in Fig. 4c.[111] This is attributed to the re-orientation of hydroxyl dipoles induced by programming-erasing bias. As a result, under −40 V gate plus, responsivity of I_{on} increases to 66.9% for 0.5 ppm NH_3 and 30.2% for 0.2 ppm NH_3, respectively.

4. Microstructure regulations of sensing layers

The organic active layers play a vital role in both charge transport and sensing of OTFT based sensors. Microstructure regulations of organic active layers are one of the most straightforward and effective methods to improve the performance of OTFT sensors. There are several microstructure regulation methods that can effectively improve the sensitivity and response rate of the devices, including adopting ultrathin OSC films, creating porous OSC films and introducing binary or ternary OSC blend films. Ultrathin and porous OSC films can effectively shorten the diffusion distance of the gas analytes from the atmosphere to the conduction channel, which can accelerate the response/recovery time and improve the sensitivity, while the OSC film blends can enhance the absorption efficiency of the active film to analytes, thereby increasing sensitivity.

4.1 Ultrathin OSC films

The thickness of the conduction channel is only about a few molecular layers in the OSC films near the interface between the OSC and dielectric. However, the thickness of the OSC films

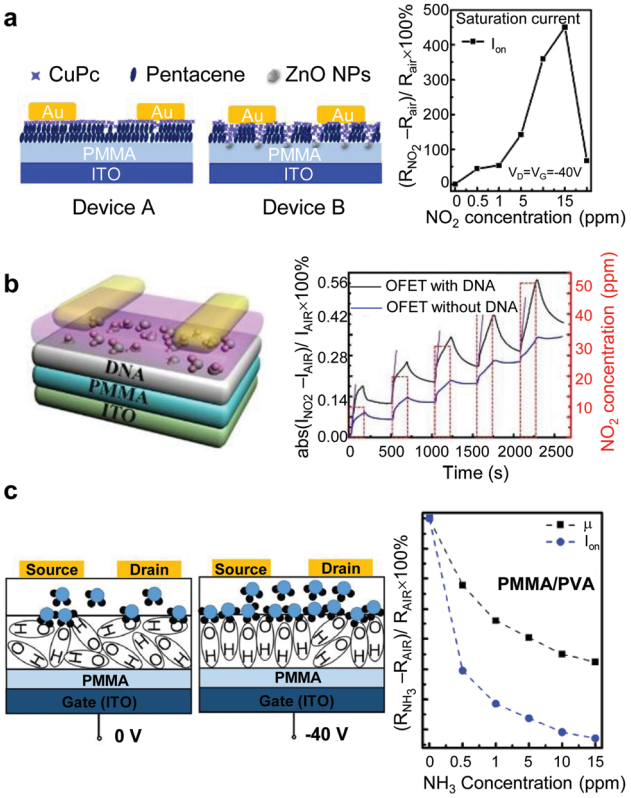

Fig. 4 Examples of dielectric modifier can interact with analyte gases directly mentioned in this review. (a) On the left is the schematic of the device structure where ZnO nanoparticles as impurities embedded in PMMA/CuPc-pentacene, and on the right is the responsivity–NO_2 concentration curve. (b) On the left is the schematic of the device structure where DNA is the interlayer and on the left are the current responsivity–time curves. (c) On the left and in the middle are the orientation schematics of hydroxyl dipoles of the gas sensor without and with bias applied, and on the right is the responsivity curves of carrier mobility and saturation current at different NH_3 concentration when −40 V gate voltage is applied on the PMMA/PVA based gas sensor. Adapted with permission from ref. 110, 74 and 111, respectively. Copyright (a) 2016 licensee MDPI Basel, Switzerland, (b) 2015 Elsevier, (c) 2016 Elsevier.

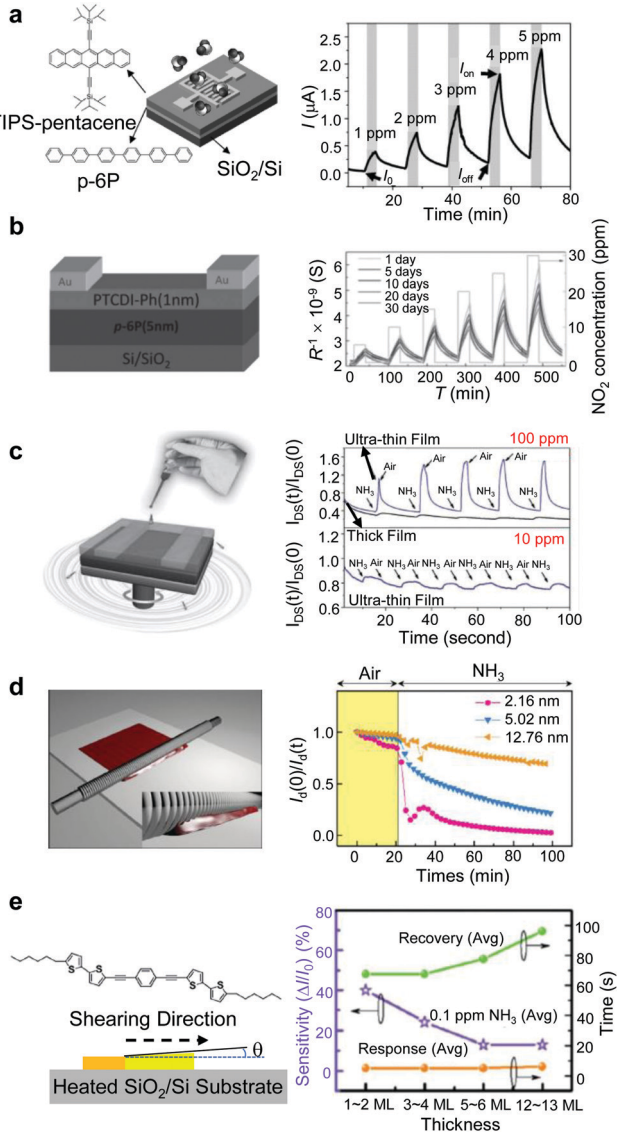

Fig. 5 Schematic illustration of the device configuration (left), and the relative response of 1 nm PTCDI-Ph, and 5 nm p-6P film to NO_2 pulses (right). (b) The configuration of the sensor (left), and dynamic response of a 7.5 nm TIPS-pentacene/p-6P film when exposed to different NO_2 concentrations (right). (c) Schematic illustration of the on-the-fly-dispensing spin-coating approach (left), and dynamic response of the NDI(2OD)(4tBuPh)-DTYM2 based film and ultrathin-film transistors to 1 and 10 ppm NH_3 under ambient conditions (right). (d) The schematic illustration of bar-coating with wound wire in the bar (left), and the normalized current response of the devices with different film thickness when exposed to NH_3 (right). (e) Schematic diagram of solution-shearing technique (left), and the sensitivity, response and recovery time of NH_3 sensors with different thickness toward 100 ppb NH_3 (right). Adapted with permission from ref. 44, 121, 122, 60 and 123, respectively. Copyright (a) 2017 Wiley, (b) 2013 Wiley, (c) 2012 Wiley, (d) 2016 Wiley and (e) 2014 The Royal Society of Chemistry.

used in OTFTs is basically tens of nanometers, which limits the diffusion of the gas analyte to the channel and may cause slow response and recovery and poor sensitivity. There are many techniques that can be considered to fabricate ultrathin OSC films, such as bar-coating,[60] thermal evaporation,[112–114] spin-coating,[114,115] drop-casting, blade-coating,[116–118] inkjet printing, spray-coating, dip-coating,[119] and self-assembly.[120] Thermal evaporation is a common fabrication technique for small-molecule OSCs, that can precisely control the thickness of OSC films in sub-nanometer scales.[36] For instance, Katz *et al.* reported ultrathin OTFTs based on the 5,5′-bis(4-hexylphenyl)-2,2′-bithiophene (6PTTP6) monolayer as the OSC sensing part, which demonstrated much greater sensitivity and faster response than devices with a thicker OSC film.[53] In a report by Wang *et al.*, ultrathin 5 nm TIPS-pentacene with high mobility was deposited on the modified SiO_2/Si substrate (Fig. 5a).[44] Both an ultrahigh sensitivity of 1000% ppm^{-1} and a calculated LOD of 20 ppb were obtained. In addition, this work systematically studied the relationship between the high sensing performance and the charge transport characteristics of the films by using different OSC materials (TIPS-pentacene and pentacene), and found that the combination of high mobility and low initial carrier concentration is a critical factor

to acquire ultrahigh sensitivity. Besides the sole material-based monolayers, ultrathin OSCs based on two-layer heterojunction structures were also developed and used in OTFT for NO_2 detection. The reported ultrathin heterojunction was deposited by thermal evaporation of *N*,*N*′-diphenyl perylene tetracarboxylic diimide (PTCDI-Ph) onto an ultrathin *para*-hexaphenyl (p-6P) film, where both PTCDI-Ph and p-6P were sensitive to NO_2 (Fig. 5b).[121] As a result, the heterojunction devices exhibited great sensitivity, recoverability, and stability.

The thermal evaporation methods can be used to easily tune the film thickness *via* controlling the deposition rate, and the obtained ultrathin film is of high-quality with low-density defects. Nevertheless, the requirement of specific vacuum equipment increases the fabrication cost and limits the large area processing. Furthermore, polymer OSCs cannot be deposited by thermal evaporation but only by solution methods. In this case, many studies have focused on the use of innovative solution methods to obtain ultrathin OSC films. Zhang *et al.* reported a simple and low-cost on-the-fly-dispensing spin-coating approach, in which a small amount of NDI(2OD)(4tBuPh)-DTYM2 solution was dropped on the high speed rotating substrate (Fig. 5c).[122] The 4 nm thick NDI(2OD)(4tBuPh)-DTYM2 ultrathin film used as a sensing layer in OTFTs showed a much higher sensitivity and faster response time to NH_3 compared with 70 nm thick NDI(2OD)(4tBuPh)-DTYM2 based OTFT sensors. Khim *et al.* reported OTFT sensors using an ultrathin DPPT-TT layer using a simple bar-coating method (Fig. 5d).[60] The corresponding devices with 2.16 nm, 5.0 nm and 12.8 nm thick DPPT-TT ultrathin films presented sensitivities of 82%, 27% and 10% to 10 ppm NH_3, respectively. As displayed in Fig. 5e, Zhu *et al.* reported high-sensitive NH_3 sensors with a solution-shearing coated ultrathin 1,4-bis((5′-hexyl-2,2′-bithiophen-5-yl)ethynyl)benzene (HTEB) film as the active layer, achieving ppb level detection capability.[123]

4.2 Porous OSC films

The porous structures in OSC active layers allow analytes to diffuse through nano/micropores to the conduction channel more easily than dense OSC films. So, creating porous structures has been widely adopted in gas sensors in recent years. Here we discuss several effective approaches for fabricating porous OSC films to improve the performance of gas sensors.

Using templates for assisting pore formation with controllable pore sizes is an effective way to develop porous OSC films. As shown in Fig. 6a, Zhang and co-workers reported the use of a nanoporous insulating layer as the template to create adjustable porous structured DPP OSC layers, where the template was prepared by adding 4,4′-(hexafluoroisopropylidene)diphthalic anhydride (HDA) into poly(4-vinylphenol) (PVP) tetrahydrofuran (THF) solution as a cross-linking agent.[61] By adjusting the HAD/PVP ratio, the diameter of the nanopores could be programmed ranging from 50 to 700 nm, and thus "printed" on the OSCs *via* meniscus-guided or spin-coating. The resulting porous sensors showed that the sensing performance was highly relevant to the pore size, and the device with average pore diameters of 700 nm exhibited the best sensing performance for NH_3 and formaldehyde with a LOD as low as 1 ppb. Similarly, Kang *et al.* deposited bis(triphenylsilyl)benzene (TSB3) on heated SiO_2 substrates to form porous templates, followed by deposition of a pentacene thin film on top as the porous OSC sensing layer.[124] Short response and recovery time are obtained by the devices with TSB3. Meanwhile, the devices show high sensitivity and stable sensing behavior. Templates "lift-off" are another effective way for creating porous OSC films. For instance, Huang *et al.* reported ultrathin porous OSC based OTFT sensors *via* deposition of a dinaphtho[2,3-*b*:2′,3′-*f*]thieno[3,2-*b*]thiophene (DNTT) OSC thin film on an SiO_2 dielectric with pre-dispersed polystyrene (PS) microspheres (Fig. 6b).[39] The microporous structures were obtained by physical removal of PS microspheres using adhesive tapes, and the size of the pores was controlled by the diameter of the PS microspheres. The resulting sensors showed great sensitivity of 340% ppm^{-1} at a ppb level of detection.

Another simple method to create porous OSC films can be realized by doping additives into the OSC films. Wang *et al.* reported the development of microporous conjugated-polymer semiconductor PBIBDF-BT films *via* blending of an insulating material poly(1,4-butylene adipate) (PBA).[125] As shown in Fig. 6c, the blend solutions were first spin-coated onto the amorphous fluoropolymer (Cytop)-treated SiO_2/Si substrate, and a phase-separation between the PBIBDF-BT and PBA occurred in the blend film. Then the microporous PBIBDF-BT films could be formed *via* simple removal of PBA using acetone. The sensors with the microporous PBIBDF-BT films exhibited greater sensitivity to NH_3 than dense PBIBDF-BT film-based devices. Zhang *et al.* fabricated porous P3HT/PS blend films by a breath figure patterning method.[126] They placed the blend film in a humid environment to allow the water vapour to condense on the film surface, resulting in solid films with a porous structure. The porous devices showed a responsivity of 280% to 10 ppm NO_2, a couple of times greater than that of the dense film-based devices.

4.3 Blend OSC films

In recent years, a large number of studies on OTFTs with OSC/polymer blend films were reported, which showed advantages of great electrical performance, good environmental stability, and remarkable mechanical properties.[127–130] These blend films can provide a large density of interfaces to interact with gas analytes, resulting in efficient detection of gases, and thus were widely applied in OTFT based gas sensors. Han *et al.* reported a NH_3 gas sensor with OSC/insulating polymer blend as the active film (Fig. 7a).[131] Phase separation of the blend film resulted in P3HT-enriched on the top of the blend film that offered effective interaction between the OSC and the gas analyte with a sensitivity of 74% to 50 ppm NH_3. Further study of the insulating polymer selection in blend films for gas sensing was carried out by the same group, and poly(9-vinylcarbazole) (PVK) was discovered to be a good candidate for the blend system (Fig. 7b).[132] Due to the increased contact area of P3HT/NH_3 and hole-transportation/electron-block effects induced by PVK, an ultra-high responsivity of ~22 000% was achieved by the P3HT/PVK blend OTFT sensor,

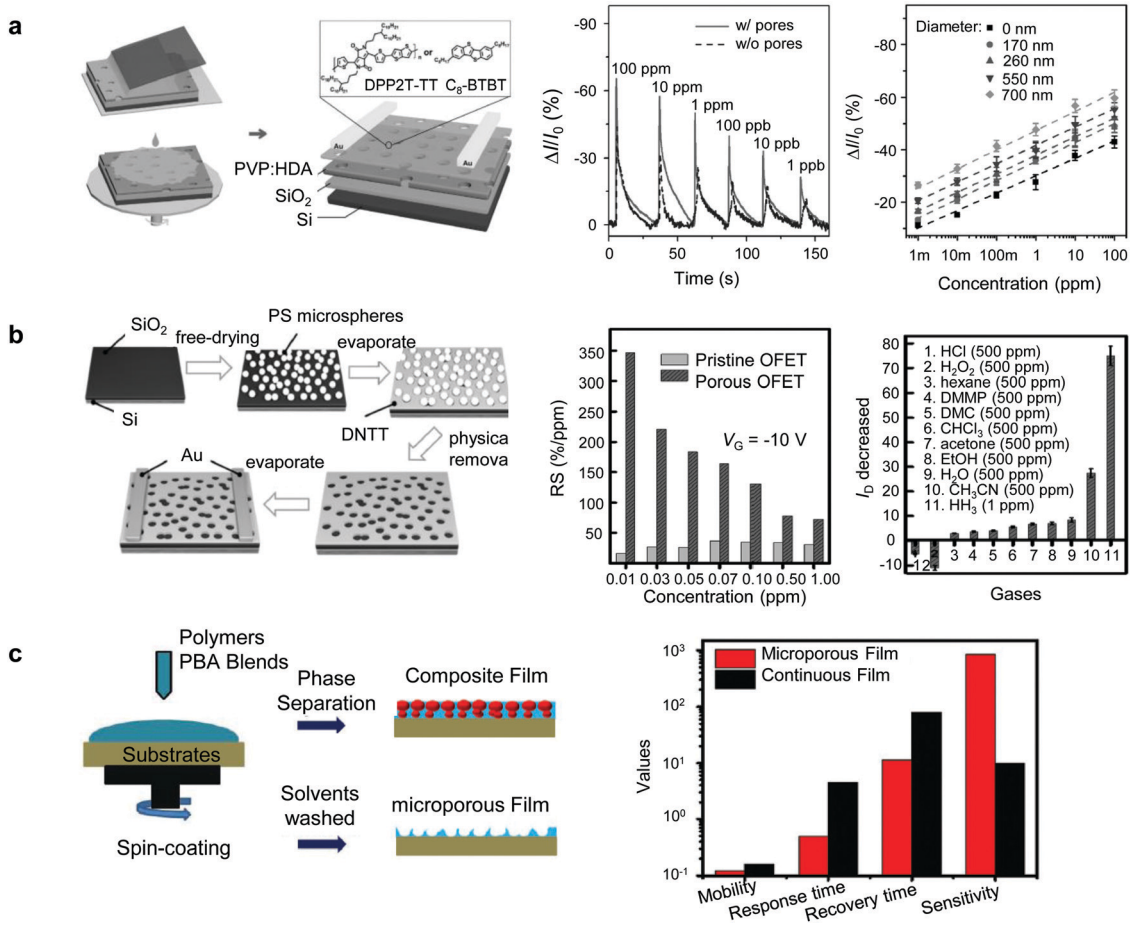

Fig. 6 Schematic illustration of nanoporous semiconductor layer formation templated by a nanoporous PVP/HDA layer *via* meniscus-guided coating and spin-coating. Also shown is the corresponding nanoporous field-effect transistor device architecture (left column). Current responses of DPP2T-TT-based sensing device with/without pores to a series of NH_3 concentrations (middle column), and current response of DPP2T-TT devices towards NH_3 with different pore sizes (right column). (b) The fabrication procedure of the porous OFET-based sensors (left column), the relative sensitivity (RS) of the pristine and porous OFET-based sensors to different concentrations of NH_3 (middle column), and response of I_D to different gases and solvent vapours (right column). (d) Schematic diagram of the microporous film fabrication process (left column), and the properties of the microporous- and continuous-film based sensors (right column). Adapted with permission from ref. 61, 39 and 125, respectively. Copyright (a) 2017 Wiley, (b) 2017 Wiley, and (c) 2016 Wiley.

which is 37 times greater than that of pure P3HT sensors. By carefully controlling the blending ratio and the solution preparation process, vertical phase separation between OSC and the insulating polymer can be realized, that allows layer by layer formation of OSCs and insulating polymers to be completed in a one-step coating. Recently, Hou *et al.* reported a simple one-step processing method *via* vertical phase separation of P3HT and poly(methyl methacrylate) (PMMA) in OTFT for NO_2 detection (Fig. 7c).[51] A large amount of micro/nano-gaps formed between P3HT and PMMA in self-stratified films resulted in an enhanced adsorption amount of NO_2. Compared to the devices obtained by the traditional two-step process, the one-step devices show similar or even better electronic performance and an improved sensitivity to NO_2, with a LOD of 0.7 ppb. In addition, the decent selectivity, environmental stability and an excellent limit of detection of 242.6 ppb were also realized by blending OSCs with poly[*N*,*N*′-bis(4-butylphenyl)-*N*,*N*′-bis(phenyl)-benzidine] (poly-TPD), exhibiting the expansive prospect of the blend films in gas sensor applications.[51]

5. Other progress in OTFT based gas sensors

Besides interfacial engineering and microstructure regulation, other efforts have also been made for developing OTFT based gas sensors. In this section, we discuss the recent advances in exploration of new biomaterials and deployment of circuits and sensor arrays for OTFT sensors with high sensitivity, high selectivity and environmental stability.

5.1 Biomaterials in OTFT based gas sensors

Biomaterials have attracted great attention in recent years as which can be used in bio-markers, bio-integrated electronics and many other fields. Biomaterials are basically organic materials, owing to the advantages of low-cost, low-toxicity, abundance, and environmental friendliness. Therefore, applying biomaterials in OTFTs is a natural step in exploring OTFTs. One of the key points of applying biomaterials in OTFTs is the compatibility between biomaterials and the other functional

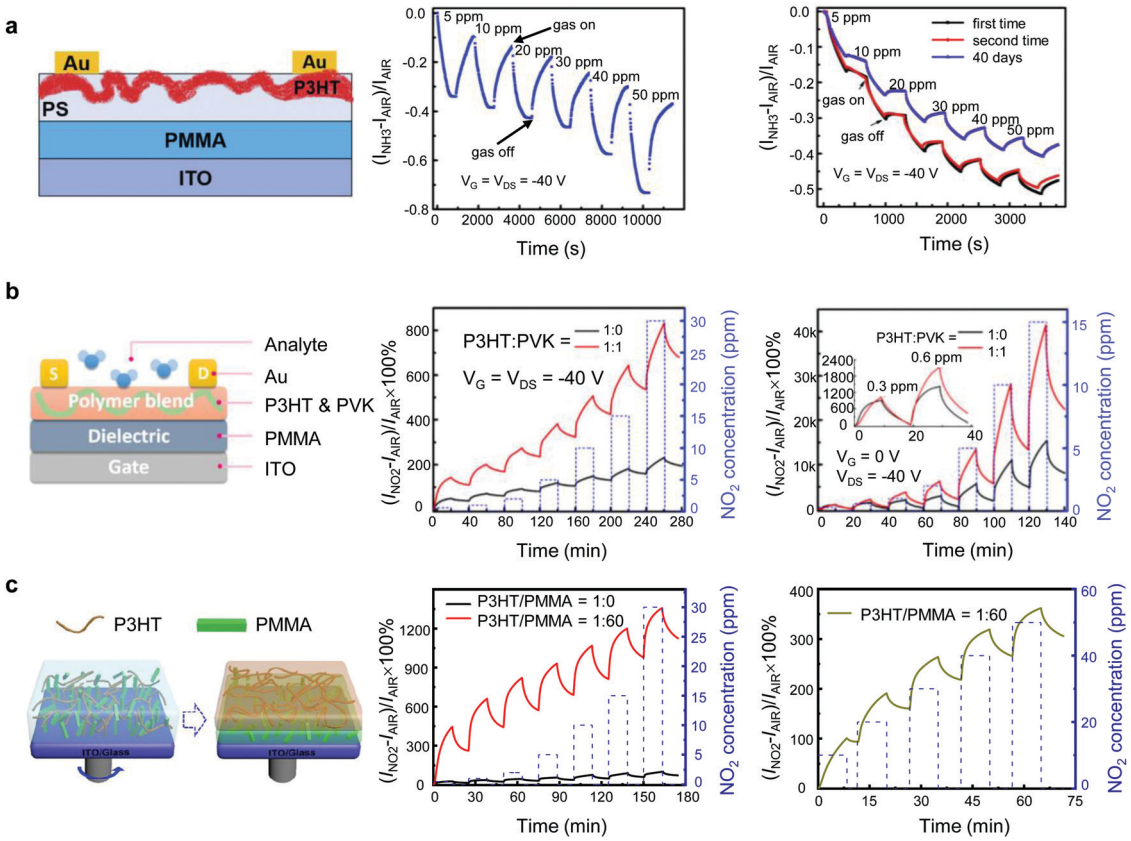

Fig. 7 (a) Schematic structure of OTFT sensors based on P3HT/PS blend films (left), real-time responsivity to dynamic NH_3 concentrations (middle), and response curves to NH_3 at different concentrations tested twice successively and after storing in the atmosphere for 40 days (right). (b) Schematic illustration of P3HT/PVK OTFT gas sensor architecture (left), and percentage change of current to dynamic NO_2 concentrations. $V_G = V_{DS} = -40$ V (middle), and $V_G = 0$ V, $V_{DS} = -40$ V (right). (c) Schematic illustrations of the fabrication process for the blend OTFT based sensors (left), percentage change of current to different NO_2 concentrations (middle), and sensitivity of the blend devices in low concentration of NO_2, and calculation of the limit of detection (right). Adapted with permission from ref. 131, 132 and 51, respectively. Copyright (a) 2016 Elsevier, (b) 2018 American Chemical Society, (c) 2019 American Chemical Society.

material in OTFTs. Guanine plays an important role in organisms in living bodies, which interestingly is an excellent dielectric material due to its low dielectric loss properties. In 2017, guanine was adopted as a functional layer in pentacene OTFTs by Shi *et al.*, where both guanine and pentacene were thermally deposited (Fig. 8a).[71] The guanine/pentacene having a layer-by-layer structure neutralized the charge traps, resulting in the enhancement of the OTFT performance compared to the pure pentacene structure. Furthermore, the guanine/pentacene OTFTs can be used as sensors for NO_2 detection with an enhanced sensitivity compared with that of pure pentacene OTFT. In addition, the two kinds of OTFTs showed different response behaviours to various gas analytes (Fig. 8a), which indicated the potential of developing OTFT sensors with great selectivity.[70] Polymeric biomaterials can also be used as functional layers in OTFT based sensors. Jang *et al.* introduced methyl cellulose (MC) as the modification layer of dielectrics for high performance pentacene OTFT based gas sensors.[38] As shown in Fig. 8b, the sensors with MC modification layer showed improved sensitivity with a shorter recovery time compared with that of sensors without MC. An increased number of grain boundaries induced by the MC buffer layer were claimed to be the reason for the enhancement of sensing performance. Gelatin, obtained from animal bones and skins, is another polymeric material that can also be used in the OTFT based sensor. Zhuang *et al.* fabricated OTFT based NH_3 sensors with gelatin as the dielectric layer (Fig. 8c).[47] The functional groups on the gelatin dielectric surface exhibited the ability to adsorb NH_3, resulting in high sensitivity.

5.2 Integrating sensor arrays

The sensor array formed by integrating a large number of OTFTs can realize advanced functions that cannot be obtained using a single OTFT device.[69] OTFT sensor arrays are excellent platforms to improve the selectivity of gas analytes. The interactions between gas analytes and different OSCs could induce corresponding responses which exhibit their own characteristics. Thus, integration of various OSC based OTFT sensors enables selective recognition of gas analytes. Crone and co-workers studied the selective detection of 16 gas analytes by using an OTFT gas sensor array, where 11 different OSCs were used as sensing layers (Fig. 9a).[133] Subsequently, Katz *et al.*

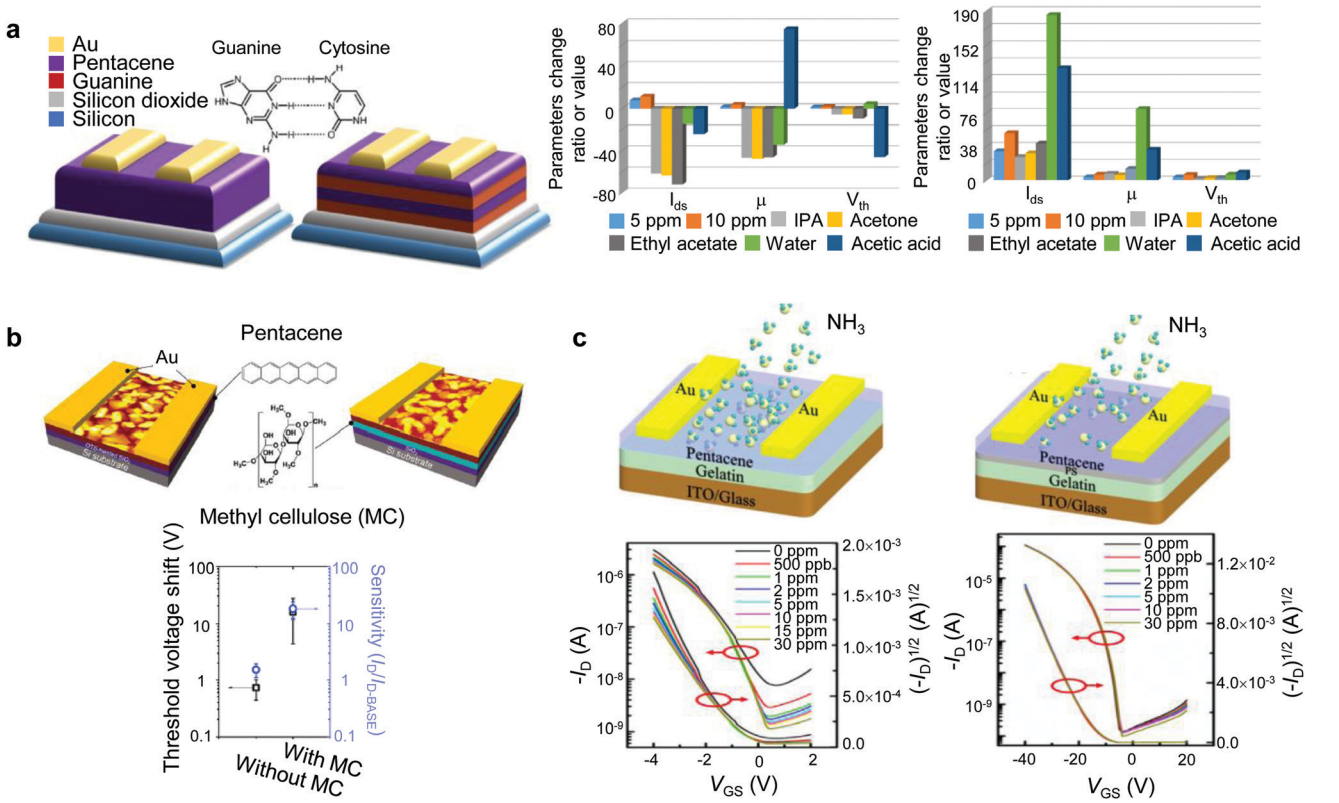

Fig. 8 (a) Schematic structure of the OTFTs with a single pentacene layer and guanine/pentacene/guanine/pentacene layer-by-layer structures, and the molecular structure of guanine. Drain current, mobility, and threshold voltage change of pentacene (middle) and pentacene/guanine (right) layer-by-layer OTFTs to 5 ppm NO_2, 10 ppm NO_2, IPA, acetone, ethyl acetate, water, and acetic acid under 5 min exposure. (b) Device schematic and molecular structures of pentacene and MC (top), and statistical comparisons of the sensitivity and threshold voltage to 20 ppm NO_2 (bottom). (c) Schematic architecture, and typical transfer curves of the NH_3 sensor with gelatin (left) and gelatin/PS (right) as the dielectric layer. Adapted with permission from ref. 71, 70, 38 and 47, respectively. Copyright (a) 2017 American Institute of Physics, 2017 Elsevier (b) 2019 The Royal Society of Chemistry, and (c) 2019 American Chemical Society.

combined the multiple detection parameters, including I_{DS}, μ, and V_{th}, with the OTFT sensor array and successfully identified 16 gases using only three kinds of OSCs (CuPc, *N*,*N*′-dioctyl naphthalenetetracarboxylic diimide (8-NTCDI), and dimethylpropylamine naphthalenetetracarboxylic diimide (DMP-NTCDI)) (Fig. 9a).[134] These results indicated the ability for selective recognition of individual analytes by introducing various OSCs into an OTFT array. In addition, many efforts have been devoted to enhance the sensitivity of OTFT based sensor array. Lee *et al.* reported 5,11-bis(triethylsilylethynyl) anthradithiophene (TES-ADT) OTFT arrays by using a solvent-containing engraved polydimethylsiloxane (PDMS) mold (Fig. 9b).[135] The number of integrated OTFTs can be controlled by changing the width of the TES-ADT pattern. The sensor array with more OTFTs offered a more effective diffusion pathway, and thus exhibited faster response/recovery rates and higher sensitivity.

OTFT based integrated circuits with unique functionalities can also be used in gas sensing. Fan *et al.* reported a poly-(bisdodecylquaterthiophene) (PQT-12)/PS based sensitive circuit for humidity-stabilized sensing, and this circuit consists of two OTFTs in series which share one gate electrode, as illustrated in Fig. 9c.[136] Furthermore, the PQT-12/PS sensitive blend film in device A was treated by UV–ozone for 10 s, whereas it was not treated in device B. Device A exhibited a sensitivity of 93% to 200 ppb NO_2, nearly 15 times greater than the devices with untreated films, which was due to the effective adsorption of NO_2 by the UV–ozone newly induced functional groups. The V_{out} of the invertor was used as the detection parameter for humidity, and a common multimeter can be used to read the sensing signal instead of semiconductor analyzers. Yuvaraja *et al.* built an analog-to-digital converter (ADC) gas detection system based on two OTFTs, where poly{3,6-dithiophen-2-yl-2,5-bis(2-decyltetradecyl)pyrrolo[3,4-*c*] pyrrole-1,4-dione-*alt*-thienylenevinylene-2,5-yl} (PDVT-10) served as the OSC (Fig. 9d).[137] The single 3D metal–organic framework (MOF)-modified devices as gas sensing blocks showed excellent sensitivity and selectivity. The gate voltage of the bottom device was tuned in five-step intervals from −7 to −25 V to control the output voltage. When the output voltage surpassed the reference voltage level, the ADC system generated either a "1" under the function of the inverting operation amplifier, otherwise a "0". Then the concentrations of target gas were quantified into digital bits.

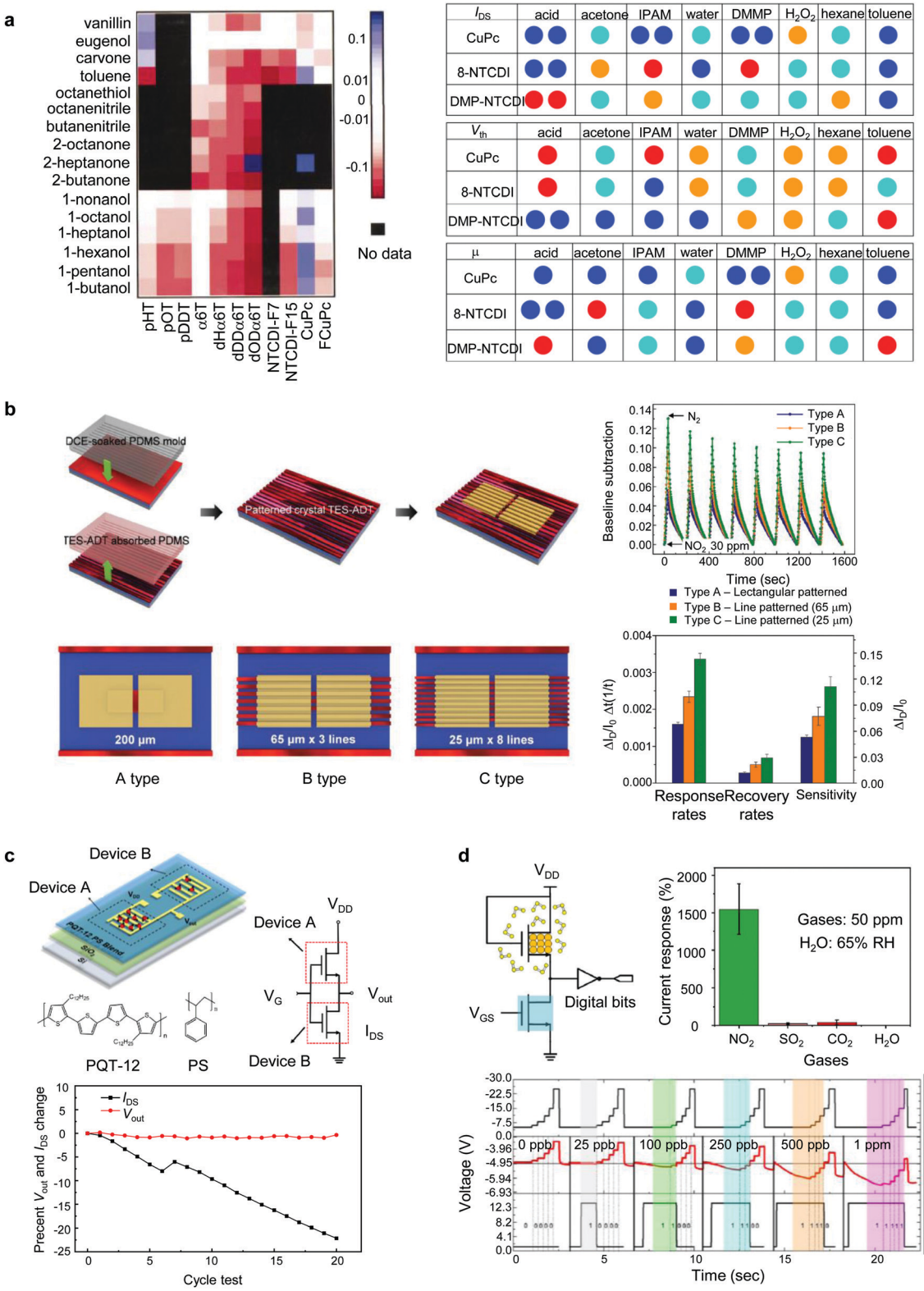

Fig. 9 (a) On the left is a map illustrating the response of 11 sensitive materials on 16 analytes. And on the right is the qualitative drain current, threshold voltage, and mobility change map of different analytes. The red spot represents a large parameter value increase, and two red spots represent a much larger increase. The blue spot represents a large parameter value decrease, and two blue spots represent a much larger decrease. The light blue spot means slight parameter value decrease, while the orange spot means a slight increase. (b) Schematic of the device fabrication process of three types of patterned TES-ADT films (left), real-time response and sensing parameters of the three types of device towards 30 ppm NH_3 (right). (c) Schematic structure of the OTFT based circuit, and the chemical structure of PQT-12 and PS (top), and percentage change of I_{DS} and V_{out} under a humid environment (bottom). (d) Schematic illustration of the ADC circuit system (upper left corner), selectivity of the 3D-MOF/PDVT-10 OTFT device (upper right corner), and transient analysis of the integrated ADC system towards different gas concentration levels (bottom). Adapted with permission from ref. 133–137, respectively. Copyright (a) 2001 American Institute of Physics and 2013 Wiley, (b) 2020 Wiley, (c) 2019 American Chemical Society, and (d) 2020 Wiley.

6. Conclusions and outlook

OTFT based gas sensors have been proven to have great potential in the field of drug delivery, food storage, fire detection, environmental monitoring, and smart health care, owing to the advantages of low cost, low temperature processability and operability, multi-parameter detectability and mechanical flexibility. The recent progress of OTFT gas sensors summarized in this review involves chemically sensitive materials, interfacial engineering, microstructure regulation of organic active layers, utilizing biomaterials, and integrating sensor arrays. Practical gas sensing applications based on OTFTs can be considered in the future by adopting the advanced strategies mentioned in this review.

Although great progress has been achieved in the past decade, there are still some challenges that limit the commercial applications of OTFT sensors. Further work may focus on the following areas: (1) further investigations of the sensing mechanisms need to be studied in detail. A specific question as to how the analytes affect the electrical parameter variations is still an X factor, since the interactions mainly happen in several parts such as between the analytes and the active materials, the grain boundaries and the dielectric surfaces. (2) There are conflicts between some electrical characteristics of the sensors. For example, the stronger interaction between analytes and devices leads to higher sensitivity but also limits the recovery rate. (3) The long-term operation stability issue is that OTFT sensors with bias can achieve a great signal-to-noise ratio, but the bias induced current draft comes behind. (4) Selectivity is an intrinsic limitation of OSCs. Even though modifying the OSCs with functional groups is an effective strategy to improve selectivity, it is not applicable for mass production, and recoverability is also a problem. Thus, more efforts are needed to focus on state-of-the-art strategies, such as integrating sensor arrays. (5) Most of the reported OTFT sensors adopted SiO_2 or polymer as dielectrics, so the high operation voltage is still a problem when considering the development of OTFT sensors into portable and wearable electronics. Overall, we hope that this review will provide a comprehensive understanding of the advances in materials science, chemistry and physics in OTFT based gas sensors, and offer inspiration and guidance to both academics and industry to explore the topmost level of sensing capacity of OTFT sensors.

Conflicts of interest

There are no conflicts to declare.

Acknowledgements

This work is supported by the National Key R&D Program of China (Grant No. 2018YFB0407102), the Foundation of the National Natural Science Foundation of China (NSFC) (Grant No. 61421002, 61675041, and 51703019), the Sichuan Science and Technology Program (Grant No. 2019YFG0121 2019YJ0178 and 2020YFH0181), and the Sichuan Province Key Laboratory of Display Science and Technology. This work is also sponsored by the Research Grants Council of the Hong Kong Special Administrative Region (Grant No. 21210820) and City University of Hong Kong (Grants No. 9610423 and 9667199). M. Wu thanks the Academic Support Program for PhD students supported by the University of Electronic Science and Technology of China.

Notes and references

1 Y. N. Li, P. Sonar, L. Murphy and W. Hong, *Energy Environ. Sci.*, 2013, **6**, 1684–1710.
2 F. Zhang, Y. Hu, T. Schuettfort, C. A. Di, X. Gao, C. R. McNeill, L. Thomsen, S. C. Mannsfeld, W. Yuan, H. Sirringhaus and D. Zhu, *J. Am. Chem. Soc.*, 2013, **135**, 2338–2349.
3 B. Sun, W. Hong, Z. Yan, H. Aziz and Y. Li, *Adv. Mater.*, 2014, **26**, 2636–2642.
4 Z. Yi, S. Wang and Y. Liu, *Adv. Mater.*, 2015, **27**, 3589–3606.
5 L. Zhu and W. Zeng, *Sens. Actuators, A*, 2017, **267**, 242–261.
6 A. Dey, *Mater. Sci. Eng., B*, 2018, **229**, 206–217.
7 A. F. Paterson, S. Singh, K. J. Fallon, T. Hodsden, Y. Han, B. C. Schroeder, H. Bronstein, M. Heeney, I. McCulloch and T. D. Anthopoulos, *Adv. Mater.*, 2018, e1801079, DOI: 10.1002/adma.201801079.
8 D. Kwak, Y. Lei and R. Maric, *Talanta*, 2019, **204**, 713–730.
9 N. Wang, A. Yang, Y. Fu, Y. Li and F. Yan, *Acc. Chem. Res.*, 2019, **52**, 277–287.
10 H. Nazemi, A. Joseph, J. Park and A. Emadi, *Sensors*, 2019, **19**, 1285.
11 H. Klauk, *Chem. Soc. Rev.*, 2010, **39**, 2643–2666.
12 X. C. Ren, F. X. Yang, X. S. Gao, S. T. Cheng, X. T. Zhang, H. L. Dong and W. P. Hu, *Adv. Energy Mater.*, 2018, **8**, 1801003.
13 N. A. Minder, S. Lu, S. Fratini, S. Ciuchi, A. Facchetti and A. F. Morpurgo, *Adv. Mater.*, 2014, **26**, 1254–1260.
14 J. Y. Oh, S. Rondeau-Gagne, Y. C. Chiu, A. Chortos, F. Lissel, G. N. Wang, B. C. Schroeder, T. Kurosawa, J. Lopez, T. Katsumata, J. Xu, C. Zhu, X. Gu, W. G. Bae, Y. Kim, L. Jin, J. W. Chung, J. B. Tok and Z. Bao, *Nature*, 2016, **539**, 411–415.
15 Y. Lee, M. Shin, K. Thiyagarajan and U. Jeong, *Macromolecules*, 2015, **49**, 433–444.
16 K. Fukuda, Y. Takeda, Y. Yoshimura, R. Shiwaku, L. T. Tran, T. Sekine, M. Mizukami, D. Kumaki and S. Tokito, *Nat. Commun.*, 2014, **5**, 4147.
17 H. T. Yi, M. M. Payne, J. E. Anthony and V. Podzorov, *Nat. Commun.*, 2012, **3**, 1259.
18 A. C. Arias, J. D. MacKenzie, I. McCulloch, J. Rivnay and A. Salleo, *Chem. Rev.*, 2010, **110**, 3–24.
19 B. Nketia-Yawson and Y.-Y. Noh, *Macromol. Res.*, 2017, **25**, 489–495.
20 W. Huang, X. Zhuang, F. S. Melkonyan, B. Wang, L. Zeng, G. Wang, S. Han, M. J. Bedzyk, J. Yu, T. J. Marks and A. Facchetti, *Adv. Mater.*, 2017, **29**, 1701706.
21 X. Yu, T. J. Marks and A. Facchetti, *Nat. Mater.*, 2016, **15**, 383–396.
22 T. Xie, G. Z. Xie, H. F. Du, Y. J. Su, Z. B. Ye, Y. Y. Chen and Y. D. Jiang, *Sens. Actuators, B*, 2016, **230**, 176–183.

23 W. Shi, X. Yu, Y. Zheng and J. Yu, *Sens. Actuators, B*, 2016, **222**, 1003–1011.
24 T. Xie, G. Z. Xie, Y. Zhou, J. L. Huang, M. Wu, Y. D. Jiang and H. L. Tai, *Chem. Phys. Lett.*, 2014, **614**, 275–281.
25 B. Y. Shao, Y. M. Liu, X. M. Zhuang, S. H. Hou, S. J. Han, X. G. Yu and J. S. Yu, *J. Mater. Chem. C*, 2019, **7**, 10196–10202.
26 Y. Yang, G. Zhang, H. Luo, J. Yao, Z. Liu and D. Zhang, *ACS Appl. Mater. Interfaces*, 2016, **8**, 3635–3643.
27 H. W. Luo, S. J. Chen, Z. T. Liu, C. Zhang, Z. X. Cai, X. Chen, G. X. Zhang, Y. S. Zhao, S. Decurtins, S. X. Liu and D. Q. Zhang, *Adv. Funct. Mater.*, 2014, **24**, 4250–4258.
28 S. Mun, Y. Park, Y. K. Lee and M. M. Sung, *Langmuir*, 2017, **33**, 13554–13560.
29 T. Someya, A. Dodabalapur, J. Huang, K. C. See and H. E. Katz, *Adv. Mater.*, 2010, **22**, 3799–3811.
30 X. Zhou, K. Niu, Z. Wang, L. Huang and L. Chi, *Nanoscale*, 2018, **10**, 8832–8839.
31 Y. Kim, T. K. An, J. Kim, J. Hwang, S. Park, S. Nam, H. Cha, W. J. Park, J. M. Baik and C. E. Park, *J. Mater. Chem. C*, 2014, **2**, 4539–4544.
32 Y. H. Yang and H. E. Katz, *J. Mater. Chem. C*, 2017, **5**, 2160–2166.
33 S. S. Liu, H. Y. Wang, X. Y. Wang, S. R. Li, H. Y. Liu, Y. L. Chen and X. Y. Li, *J. Mater. Chem. C*, 2019, **7**, 424–433.
34 B. Nketia-Yawson, A. R. Jung, Y. Noh, G. S. Ryu, G. D. Tabi, K. K. Lee, B. S. Kim and Y. Y. Noh, *ACS Appl. Mater. Interfaces*, 2017, **9**, 7322–7330.
35 S. Chakravarty, A. Datta and N. Sen Sarma, *J. Mater. Chem. C*, 2017, **5**, 2871–2882.
36 M. Mirza, J. W. Wang, D. X. Li, S. A. Arabi and C. Jiang, *ACS Appl. Mater. Interfaces*, 2014, **6**, 5679–5684.
37 E. N. Kaya, A. Senocak, D. D. Klyamer, E. Demirbas, T. V. Basova and M. Durmus, *J. Mater. Sci.: Mater. Electron.*, 2019, **30**, 7543–7551.
38 M. Jang, S. K. Kim, J. Lee, S. Ji, W. Song, S. Myung, J. Lim, S. S. Lee, H. K. Jung, J. Lee and K. S. An, *J. Mater. Chem. C*, 2019, **7**, 14504–14510.
39 J. J. Lu, D. P. Liu, J. C. Zhou, Y. L. Chu, Y. T. Chen, X. H. Wu and J. Huang, *Adv. Funct. Mater.*, 2017, **27**, 1700018.
40 X. N. Zhang, B. H. Wang, L. Z. Huang, W. Huang, Z. Wang, W. G. Zhu, Y. Chen, Y. L. Mao, A. Facchetti and T. J. Marks, *Sci. Adv.*, 2020, **6**, eaaz1042.
41 E. L. Papadopoulou, D. Morselli, M. Prato, A. Barcellona, A. Athanassiou and I. S. Bayer, *J. Mater. Chem. C*, 2016, **4**, 7790–7797.
42 Y. Y. Mao, Q. Zhao, J. C. Wu, T. T. Pan, B. P. Zhou and Y. Q. Tian, *J. Mater. Chem. C*, 2017, **5**, 11395–11402.
43 T. Mukhopadhyaya, J. S. Wagner, H. D. Fan and H. E. Katz, *ACS Appl. Mater. Interfaces*, 2020, **12**, 21974–21984.
44 Z. Wang, L. Z. Huang, X. F. Zhu, X. Zhou and L. F. Chi, *Adv. Mater.*, 2017, **29**, 1703192.
45 W. Huang, X. M. Zhuang, F. S. Melkonyan, B. H. Wang, L. Zeng, G. Wang, S. J. Han, M. J. Bedzyk, J. S. Yu, T. J. Marks and A. Facchetti, *Adv. Mater.*, 2017, **29**, 1701706.
46 H. Li, J. Dailey, T. Kale, K. Besar, K. Koehler and H. E. Katz, *ACS Appl. Mater. Interfaces*, 2017, **9**, 20501–20507.
47 X. M. Zhuang, D. Y. Zhang, X. L. Wang, X. G. Yu and J. S. Yu, *Appl. Phys. Lett.*, 2018, **113**, 263301.
48 K. Besar, J. Dailey, X. G. Zhao and H. E. Katz, *J. Mater. Chem. C*, 2017, **5**, 6506–6511.
49 W. G. Huang, K. Besar, R. LeCover, A. M. Rule, P. N. Breysse and H. E. Katz, *J. Am. Chem. Soc.*, 2012, **134**, 14650–14653.
50 Y. Yang, G. X. Zhang, H. W. Luo, J. J. Yao, Z. T. Liu and D. Q. Zhang, *ACS Appl. Mater. Interfaces*, 2016, **8**, 3635–3643.
51 S. H. Hou, J. S. Yu, X. M. Zhuang, D. F. Li, Y. M. Liu, Z. Gao, T. Y. Sun, F. Wang and X. E. Yu, *ACS Appl. Mater. Interfaces*, 2019, **11**, 44521–44527.
52 R. D. Yang, J. Park, C. N. Colesniuc, I. K. Schuller, J. E. Royer, W. C. Trogler and A. C. Kummel, *J. Chem. Phys.*, 2009, **130**, 164703.
53 J. Huang, J. Sun and H. E. Katz, *Adv. Mater.*, 2008, **20**, 2567–2572.
54 T. Shaymurat, Q. X. Tang, Y. H. Tong, L. Dong and Y. C. Liu, *Adv. Mater.*, 2013, **25**, 2269–2273.
55 A. F. Lv, M. Wang, Y. D. Wang, Z. S. Bo and L. F. Chi, *Chem. – Eur. J.*, 2016, **22**, 3654–3659.
56 S. Tiwari, A. K. Singh, S. K. Balasubramanian, W. Takashima and R. Prakash, *J. Nanosci. Nanotechnol.*, 2016, **16**, 9634–9641.
57 P. Lienerth, S. Fall, P. Leveque, U. Soysal and T. Heiser, *Sens. Actuators, B*, 2016, **225**, 90–95.
58 M. Z. Dai, Y. L. Lin, H. C. Lin, H. W. Zan, K. T. Chang, H. F. Meng, J. W. Liao, M. J. Tsai and H. Cheng, *Anal. Chem.*, 2013, **85**, 3110–3117.
59 K. Besar, J. Dailey and H. E. Katz, *ACS Appl. Mater. Interfaces*, 2017, **9**, 1173–1177.
60 D. Khim, G. S. Ryu, W. T. Park, H. Kim, M. Lee and Y. Y. Noh, *Adv. Mater.*, 2016, **28**, 2752–2759.
61 F. J. Zhang, G. Qu, E. Mohammadi, J. G. Mei and Y. Diao, *Adv. Funct. Mater.*, 2017, **27**, 1701117.
62 J. S. Lee, S. K. Son, S. Song, H. Kim, D. R. Lee, K. Kim, M. J. Ko, D. H. Choi, B. Kim and J. H. Cho, *Chem. Mater.*, 2012, **24**, 1316–1323.
63 B. Wang, T. P. Huynh, W. Wu, N. Hayek, T. T. Do, J. C. Cancilla, J. S. Torrecilla, M. M. Nahid, J. M. Colwell, O. M. Gazit, S. R. Puniredd, C. R. McNeill, P. Sonar and H. Haick, *Adv. Mater.*, 2016, **28**, 4012–4018.
64 H. Li, J. Dailey, T. Kale, K. Besar, K. Koehler and H. E. Katz, *ACS Appl. Mater. Interfaces*, 2017, **9**, 20501–20507.
65 J. C. Bijleveld, A. P. Zoombelt, S. G. J. Mathijssen, M. M. Wienk, M. Turbiez, D. M. de Leeuw and R. A. J. Janssen, *J. Am. Chem. Soc.*, 2009, **131**, 16616–16617.
66 B. Nketia-Yawson, A. R. Jung, Y. Noh, G. S. Ryu, G. D. Tabi, K. K. Lee, B. Kim and Y. Y. Noh, *ACS Appl. Mater. Interfaces*, 2017, **9**, 7322–7330.
67 S. Wang, J. Xu, W. Wang, G.-J. N. Wang, R. Rastak, F. Molina-Lopez, J. W. Chung, S. Niu, V. R. Feig, J. Lopez, T. Lei, S.-K. Kwon, Y. Kim, A. M. Foudeh, A. Ehrlich, A. Gasperini, Y. Yun, B. Murmann, J. B. H. Tok and Z. Bao, *Nature*, 2018, **555**, 83–88.
68 T. Sakanoue and H. Sirringhaus, *Nat. Mater.*, 2010, **9**, 736–740.

69 J. Yu, X. Yu, L. Zhang and H. Zeng, *Sens. Actuators, B*, 2012, **173**, 133–138.
70 W. Shi, J. S. Yu and H. E. Katz, *Sens. Actuators, B*, 2018, **254**, 940–948.
71 W. Shi, Y. F. Zheng, A. D. Taylor, J. S. Yu and H. E. Katz, *Appl. Phys. Lett.*, 2017, **111**, 043301.
72 S. Han, W. Huang, W. Shi and J. Yu, *Sens. Actuators, B*, 2014, **203**, 9–16.
73 T. Minakata, *Polym. Adv. Technol.*, 1995, **6**, 607–610.
74 W. Shi, X. E. Yu, Y. F. Zheng and J. S. Yu, *Sens. Actuators, B*, 2016, **222**, 1003–1011.
75 X. Yu, N. Zhou, S. Han, H. Lin, D. B. Buchholz, J. Yu, R. P. H. Chang, T. J. Marks and A. Facchetti, *J. Mater. Chem. C*, 2013, **1**, 6532–6535.
76 X. Zhuang, S. Han, B. Huai, W. Shi and J. Yu, *Sens. Actuators, B*, 2019, **279**, 238–244.
77 H. Laurs and G. Heiland, *Thin Solid Films*, 1987, **149**, 129–142.
78 Z. Q. Song, G. M. Liu, Q. X. Tang, X. L. Zhao, Y. H. Tong and Y. C. Liu, *Org. Electron.*, 2017, **48**, 68–76.
79 S. Kumar, N. Kaur, A. K. Sharma, A. Mahajan and R. K. Bedi, *RSC Adv.*, 2017, **7**, 25229–25236.
80 L. S. Chia, Y. H. Du, S. Palale and P. S. Lee, *ACS Omega*, 2019, **4**, 10388–10395.
81 A. Kumar, N. Joshi, S. Samanta, A. Singh, A. K. Debnath, A. K. Chauhan, M. Roy, R. Prasad, K. Roy, M. M. Chehimi, D. K. Aswal and S. K. Gupta, *Sens. Actuators, B*, 2015, **206**, 653–662.
82 L. Wang, L. Wang, G. Yang, Q. Xie, S. Zhong, X. Su, Y. Hou and B. Zhang, *Langmuir*, 2020, **36**, 4532–4539.
83 H. Minemawari, T. Yamada, H. Matsui, J. Tsutsumi, S. Haas, R. Chiba, R. Kumai and T. Hasegawa, *Nature*, 2011, **475**, 364–367.
84 Y. W. He, M. Sezen, D. W. Zhang, A. Y. Li, L. J. Yan, H. T. Yu, C. He, O. Goto, Y. L. Loo and H. Meng, *Adv. Electron. Mater.*, 2016, **2**, 1600179.
85 A. A. Trul, A. S. Sizov, V. P. Chekusova, O. V. Borshchev, E. V. Agina, M. A. Shcherbina, A. V. Bakirov, S. N. Chvalun and S. A. Ponomarenko, *J. Mater. Chem. C*, 2018, **6**, 9649–9659.
86 Q. J. Wang, J. Qian, Y. Li, Y. H. Zhang, D. W. He, S. Jiang, Y. Wang, X. R. Wang, L. J. Pan, J. Z. Wang, X. Z. Wang, Z. Hu, H. Y. Nan, Z. H. Ni, Y. D. Zheng and Y. Shi, *Adv. Funct. Mater.*, 2016, **26**, 3191–3198.
87 Y. Tsutsui, G. Schweicher, B. Chattopadhyay, T. Sakurai, J. B. Arlin, C. Ruzie, A. Aliev, A. Ciesielski, S. Colella, A. R. Kennedy, V. Lemaur, Y. Olivier, R. Hadji, L. Sanguinet, F. Castet, S. Osella, D. Dudenko, D. Beljonne, J. Cornil, P. Samori, S. Seki and Y. H. Geerts, *Adv. Mater.*, 2016, **28**, 7106–7114.
88 F. X. Werkmeister and B. A. Nickel, *Org. Electron.*, 2016, **39**, 113–117.
89 L. Li, P. Gao, M. Baumgarten, K. Mullen, N. Lu, H. Fuchs and L. Chi, *Adv. Mater.*, 2013, **25**, 3419–3425.
90 T. Zhu, C. Xiao, B. Wang, X. Hu, Z. Wang, J. Fan, L. Huang, D. Yan and L. Chi, *Langmuir*, 2016, **32**, 9109–9117.
91 D. He, J. Qiao, L. Zhang, J. Wang, T. Lan, J. Qian, Y. Li, Y. Shi, Y. Chai, W. Lan, L. K. Ono, Y. Qi, J. B. Xu, W. Ji and X. Wang, *Sci. Adv.*, 2017, **3**, e1701186.
92 C. Liu, C. Xiao, Y. Li, W. Hu, Z. Li and Z. Wang, *Chem. Commun.*, 2014, **50**, 12462–12464.
93 H. E. Katz, A. J. Lovinger, J. Johnson, C. Kloc, T. Siegrist, W. Li, Y. Y. Lin and A. Dodabalapur, *Nature*, 2000, **404**, 478–481.
94 H. E. Katz, J. Johnson, A. J. Lovinger and W. J. Li, *J. Am. Chem. Soc.*, 2000, **122**, 7787–7792.
95 Y. Zang, F. Zhang, D. Huang, C. A. Di, Q. Meng, X. Gao and D. Zhu, *Adv. Mater.*, 2014, **26**, 2862–2867.
96 Y. Zang, D. Huang, C. A. Di and D. Zhu, *Adv. Mater.*, 2016, **28**, 4549–4555.
97 T. Shaymurat, Q. Tang, Y. Tong, L. Dong and Y. Liu, *Adv. Mater.*, 2013, **25**, 2269–2273.
98 Y. W. Huang, W. G. Zhang, H. Y. Zhai and C. L. Li, *J. Mater. Chem. C*, 2015, **3**, 466–472.
99 G. Li, D. Li, X. Liu, H. Xu, J. Zhang, S. Wang, Z. Liu and B. Tang, *Chem. Commun.*, 2019, **55**, 9661–9664.
100 Anonymous, The interface is still the device, *Nat. Mater.*, 2012, **11**, 91.
101 F. C. Grozema and L. D. A. Siebbeles, *Int. Rev. Phys. Chem.*, 2008, **27**, 87–138.
102 G. Lu, H. Usta, C. Risko, L. Wang, A. Facchetti, M. A. Ratner and T. J. Marks, *J. Am. Chem. Soc.*, 2008, **130**, 7670–7685.
103 Y. Don Park, J. A. Lim, H. S. Lee and K. Cho, *Mater. Today*, 2007, **10**, 46–54.
104 Y. Sun, Q. Xie, Y. Zhu, L. Wang, Q. Sun and L. Wang, *Appl. Surf. Sci.*, 2020, **505**, 144436.
105 L. Jiang, J. Liu, X. Lu, L. Fu, Y. Shi, J. Zhang, X. Zhang, H. Geng, Y. Hu, H. Dong, L. Jiang, J. Yu and W. Hu, *J. Mater. Chem. C*, 2018, **6**, 2419–2423.
106 D. H. Kim, H. S. Lee, H. Yang, L. Yang and K. Cho, *Adv. Funct. Mater.*, 2008, **18**, 1363–1370.
107 M. Yoshida, S. Uemura, T. Kodzasa, T. Kamata, M. Matsuzawa and T. Kawai, *Synth. Met.*, 2003, **137**, 967–968.
108 F. S. Kim, D.-K. Hwang, B. Kippelen and S. A. Jenekhe, *Appl. Phys. Lett.*, 2011, **99**, 173303.
109 A. Khassanov, H. G. Steinruck, T. Schmaltz, A. Magerl and M. Halik, *Acc. Chem. Res.*, 2015, **48**, 1901–1908.
110 S. Han, J. Cheng, H. Fan, J. Yu and L. Li, *Sensors*, 2016, **16**, 1763.
111 S. J. Han, X. M. Zhuang, Y. M. Jiang, X. Yang, L. Li and J. S. Yu, *Sens. Actuators, B*, 2017, **243**, 1248–1254.
112 Y. Jiang, W. Huang, X. Zhuang, Y. Tang and J. Yu, *Mater. Sci. Eng., B*, 2017, **226**, 107–113.
113 S. Ji, X. Wang, C. Liu, H. Wang, T. Wang and D. Yan, *Org. Electron.*, 2013, **14**, 821–826.
114 J. Huang, J. Miragliotta, A. Becknell and H. E. Katz, *J. Am. Chem. Soc.*, 2007, **129**, 9366–9376.
115 J. Huang, T. J. Dawidczyk, B. J. Jung, J. Sun, A. F. Mason and H. E. Katz, *J. Mater. Chem.*, 2010, **20**, 2644–2650.
116 J. O. Kim, J. C. Lee, M. J. Kim, H. Noh, H. I. Yeom, J. B. Ko, T. H. Lee, S. H. Ko Park, D. P. Kim and S. Park, *Adv. Mater.*, 2018, **30**, 1800647.

117 G. Giri, D. M. DeLongchamp, J. Reinspach, D. A. Fischer, L. J. Richter, J. Xu, S. Benight, A. Ayzner, M. Q. He, L. Fang, G. Xue, M. F. Toney and Z. N. Bao, *Chem. Mater.*, 2015, **27**, 2350–2359.
118 F. Molina-Lopez, H. P. Yan, X. D. Gu, Y. Kim, M. F. Toney and Z. N. Bao, *Adv. Funct. Mater.*, 2017, **27**, 1605503.
119 Z. M. Chai, S. A. Abbasi and A. A. Busnaina, *ACS Appl. Mater. Interfaces*, 2018, **10**, 18123–18130.
120 A. M. Andringa, M. J. Spijkman, E. C. P. Smits, S. G. J. Mathijssen, P. A. van Hal, S. Setayesh, N. P. Willard, O. V. Borshchev, S. A. Ponomarenko, P. W. M. Blom and D. M. de Leeuw, *Org. Electron.*, 2010, **11**, 895–898.
121 S. Ji, H. Wang, T. Wang and D. Yan, *Adv. Mater.*, 2013, **25**, 1755–1760.
122 F. J. Zhang, C. A. Di, N. Berdunov, Y. Y. Hu, Y. B. Hu, X. K. Gao, Q. Meng, H. Sirringhaus and D. B. Zhu, *Adv. Mater.*, 2013, **25**, 1401–1407.
123 Q. Meng, F. J. Zhang, Y. P. Zang, D. Z. Huang, Y. Zou, J. Liu, G. Y. Zhao, Z. R. Wang, D. Y. Ji, C. A. Di, W. P. Hu and D. B. Zhu, *J. Mater. Chem. C*, 2014, **2**, 1264–1269.
124 B. Kang, M. Jang, Y. Chung, H. Kim, S. K. Kwak, J. H. Oh and K. Cho, *Nat. Commun.*, 2014, **5**, 4752.
125 Q. H. Wang, S. H. Wu, F. Ge, G. B. Zhang, H. B. Lu and L. Z. Qiu, *Adv. Mater. Interfaces*, 2016, **3**, 1600518.
126 X. N. Zhang, B. H. Wang, L. Z. Huang, W. Huang, Z. Wang, W. G. Zhu, Y. Chen, Y. L. Mao, A. Facchetti and T. J. Marks, *Sci. Adv.*, 2020, **6**, eaaz1042.
127 C. Jiang, H. W. Choi, X. Cheng, H. Ma, D. Hasko and A. Nathan, *Science*, 2019, **363**, 719–723.
128 A. Gumyusenge, D. T. Tran, X. Luo, G. M. Pitch, Y. Zhao, K. A. Jenkins, T. J. Dunn, A. L. Ayzner, B. M. Savoie and J. Mei, *Science*, 2018, **362**, 1131–1134.
129 X. Jia, C. Fuentes-Hernandez, C.-Y. Wang, Y. Park and B. Kippelen, *Sci. Adv.*, 2018, **4**, eaao1705.
130 X. Yu, L. Zeng, N. Zhou, P. Guo, F. Shi, D. B. Buchholz, Q. Ma, J. Yu, V. P. Dravid, R. P. Chang, M. Bedzyk, T. J. Marks and A. Facchetti, *Adv. Mater.*, 2015, **27**, 2390–2399.
131 S. J. Han, X. M. Zhuang, W. Shi, X. Yang, L. Li and J. S. Yu, *Sens. Actuators, B*, 2016, **225**, 10–15.
132 S. Han, Z. Yang, Z. Li, X. Zhuang, D. Akinwande and J. Yu, *ACS Appl. Mater. Interfaces*, 2018, **10**, 38280–38286.
133 B. Crone, A. Dodabalapur, A. Gelperin, L. Torsi, H. E. Katz, A. J. Lovinger and Z. Bao, *Appl. Phys. Lett.*, 2001, **78**, 2229–2231.
134 W. Huang, J. Sinha, M.-L. Yeh, J. F. M. Hardigree, R. LeCover, K. Besar, A. M. Rule, P. N. Breysse and H. E. Katz, *Adv. Funct. Mater.*, 2013, **23**, 4094–4104.
135 D. H. Kwak, Y. Seo, J. E. Anthony, S. Kim, J. Hur, H. Chae, H. J. Park, B. G. Kim, E. Lee, S. Ko and W. H. Lee, *Adv. Mater. Interfaces*, 2020, **7**, 1901696.
136 H. Fan, H. Li, J. Han, N. McKeever, J. Yu and H. E. Katz, *ACS Sens.*, 2019, **4**, 3240–3247.
137 S. Yuvaraja, S. G. Surya, M. T. Vijjapu, V. Chernikova, O. Shekhah, M. Eddaoudi and K. N. Salama, *Phys. Status Solidi RRL*, 2020, **14**, 2000086.

